Joint CFO and Channel Estimation for RIS-aided Multi-user Massive MIMO Systems

Sumin Jeong, *Graduate Student Member, IEEE,* Arman Farhang, *Member, IEEE,* Nemanja Stefan Perović, *Member, IEEE,* and Mark F. Flanagan, *Senior Member, IEEE*

***Abstract*—Accurate channel estimation is essential to achieve the performance gains promised by the use of reconfigurable intelligent surfaces (RISs) in wireless communications. In the uplink of multi-user orthogonal frequency division multiple access (OFDMA) systems, synchronization errors such as carrier frequency offsets (CFOs) can significantly degrade the channel estimation performance. This becomes more critical in RIS-aided communications, as the RIS phases are adjusted based on the channel estimates and even a small channel estimation error leads to a significant performance loss. Motivated by this, we propose a joint CFO and channel estimation method for RIS-aided multi-user massive multiple-input multiple-output (MIMO) systems. Our proposed pilot structure makes it possible to accurately estimate the CFOs without multi-user interference (MUI), using the same pilot resources for both CFO estimation *and* channel estimation. For optimization of the RIS phase shifts at the data transmission stage, we propose a projected gradient method (PGM) which achieves the same performance as a more computationally demanding grid search technique while having a significantly lower computational complexity. Simulation results demonstrate that the proposed method provides an improvement in the normalized mean-square error (NMSE) of channel estimation as well as in the bit error rate (BER) performance. Moreover, analyzing the computational complexity and the pilot resource efficiency of the proposed method, we demonstrate that the proposed estimation approach requires low computational load and no extra cost in pilot overhead.**

***Index Terms*—Reconfigurable intelligent surface (RIS), massive MIMO, channel estimation, carrier frequency offset (CFO), CFO estimation, RIS optimization.**

I. Introduction

MASSIVE multiple-input multiple-output (MIMO) systems utilize a large number of antennas at the base station (BS) to increase the capacity of multi-user communication networks. Compared to standard MIMO systems, massive MIMO can improve the channel capacity by orders of magnitude without requiring a larger amount of spectrum [1]–[3]. However, the performance gains of massive MIMO are ultimately dependent on the stochastic nature of the wireless communication channel, which is in general a harsh propagation environment. Also, the blockage in millimeter wave (mmWave) bands where even massive MIMO cannot provide coverage to the users is another major issue. *Reconfigurable intelligent surfaces* (RISs) can be used to enhance the received signal quality, as well as to enable connectivity when the direct link is blocked [4]–[6]. An RIS is a thin metamaterial sheet which consists of a large number of passive reflecting elements. Each RIS element can control the reflections of the impinging radio waves to optimize a desirable performance metric such as the achievable rate [7]–[9]. Moreover, an RIS is a nearly-passive and highly energy-efficient structure without active electronic components (e.g., radio frequency (RF) chains). It works in a full-duplex mode without using costly self-interference cancellation or active relaying/beamforming techniques [4]. However, the optimal RIS reflection design requires close to perfect knowledge of the channel impulse response (CIR). Thus, highly accurate channel estimation is of paramount importance in RIS-aided communication networks.

Several channel estimation methods for RIS-assisted wireless communications have been proposed in the literature [10]–[21]. In [10]–[12], on/off methods estimate the channel by switching on only one RIS element at a time. However, since multiple pilot resources are required to estimate the channel for each RIS element and the RIS usually contains a large number of reflection elements, the resulting channel estimates for all RIS elements can become outdated. On the other hand, RIS reflection pattern based methods [13]–[15] use a known set of well-designed RIS reflection coefficients to simultaneously estimate all channels between the BS and the RIS. In [16]–[18], the RIS is equipped with a small fraction of active elements which can estimate useful parameters such as angle-of-arrival (AoA) or can conduct additional signal processing at each RIS element besides passive phase shifting; however, extra hardware and energy costs are required for using the active RIS elements. Channel estimation performance can be improved using deep learning [18]–[20]; however, such algorithms can incur a lengthy training time. In [21] a codebook-based approach was proposed in which, based on initial estimation of a superposition of the direct and reflected channels, one of a finite set of pre-designed RIS phase shift matrices was selected in order to optimize the achievable rate. However, this method is designed to work in flat-fading channels and is not directly implementable in frequency selective channels. Also, since it is

S. Jeong and M. F. Flanagan are with the School of Electrical and Electronic Engineering, University College Dublin, Belfield, Dublin 4, D04 V1W8 Ireland (e-mail: sumin.jeong@ucdconnect.ie; mark.flanagan@ieee.org).

A. Farhang is with the Department of Electronic and Electrical Engineering, Trinity College Dublin (TCD), College Green, Dublin 2, D02 PN40 Ireland (e-mail: arman.farhang@tcd.ie).

N. S. Perović is with Université Paris-Saclay, CNRS, CentraleSupélec, Laboratoire des Signaux et Systèmes, 3 Rue Joliot-Curie, 91192 Gif-sur-Yvette, France. (e-mail: nemanja-stefan.perovic@centralesupelec.fr).

The work of S. Jeong and M. F. Flanagan was supported by the Irish Research Council (IRC) under grants GOIPG/2018/2983 and IRCLA/2017/209. The work of A. Farhang was supported by Science Foundation Ireland (SFI) under grants 19/FFP/7005(T) and 21/US/3757. The work of N. S. Perović was supported by the European Commission through the H2020 SURFER project under grant agreement number 101030536. For the purpose of Open Access, the authors have applied a CC BY public copyright licence to any Author Accepted Manuscript version arising from this submission.

designed for downlink (DL) transmission, an additional feedback link is required to transmit the CIR obtained at the users to the BS. The aforementioned channel estimation methods provide tradeoffs between accuracy, pilot/training overhead, computational complexity, and other metrics. However, with the exception of [15], synchronization errors have not been considered in these existing channel estimation methods. Timing offsets and frequency offsets are the main synchronization errors. Timing offsets can be easily resolved by inserting a sufficiently large guard period or cyclic prefix (CP) between orthogonal frequency division multiplexing (OFDM) symbols. In contrast, frequency synchronization errors are more difficult to mitigate.

Carrier frequency offset (CFO) is an offset error between the carrier frequency of a local node and that of a reference node. If not accurately estimated and compensated, CFO can lead to significant performance degradation. This is especially true for OFDM and orthogonal frequency-division multiple access (OFDMA) systems, which are highly sensitive to the presence of CFO [15], [22]. By causing inter-carrier interference (ICI) and multi-user interference (MUI), CFOs degrade the performance of channel estimation methods that assume orthogonality between different subcarriers. If the number of unknown channels to be estimated is large, the aforementioned channel estimation methods for RIS-aided communication systems require a long pilot overhead. Therefore, when existing CFO estimation methods are used (i.e., using an additional overhead for CFO estimation), the pilot resource efficiency can be low. Therefore, efficient CFO and channel estimation methods with high pilot efficiency are of high importance for multi-carrier transmission in RIS-aided networks. In [15], the authors proposed a method for CFO estimation in RIS-aided single-user OFDM systems. However, to the best of the authors' knowledge, CFO estimation for multi-user OFDM systems equipped with an RIS has not been previously studied in the literature.

Against this background, the contributions of this paper can be summarized as follows:

- We demonstrate the detrimental effect of multiple CFOs on the channel estimation accuracy in RIS-assisted multi-user wireless networks. An important finding of this work is that even a very small amount of CFO leads to severe performance degradation, and that this escalates as the number of RIS elements increases.
- To solve this problem, we propose a joint CFO and CIR estimation technique with a high accuracy. The proposed technique does not require any additional signaling overhead for CFO estimation apart from what is required for channel estimation. We derive a closed-form expression for the mean-square error (MSE) achieved by our proposed CIR estimation method, the correctness of which is validated using numerical results.
- To evaluate the performance of the proposed estimation method, we compare it with two prominent benchmarks from the literature, namely the CIR estimation method of [14], and the joint CFO and CIR estimation method of [15] used with time-division multiple access (TDMA). It is demonstrated that the proposed estimation technique has an improved normalized mean-square error (NMSE) performance with lower computational complexity and a lower pilot overhead than these other approaches.
- We propose a projected gradient method (PGM) for optimizing the RIS phase shifts after joint CFO and CIR estimation. We show that the proposed PGM requires a significantly lower computational complexity to reach a locally optimal achievable rate than the computationally demanding grid search technique.

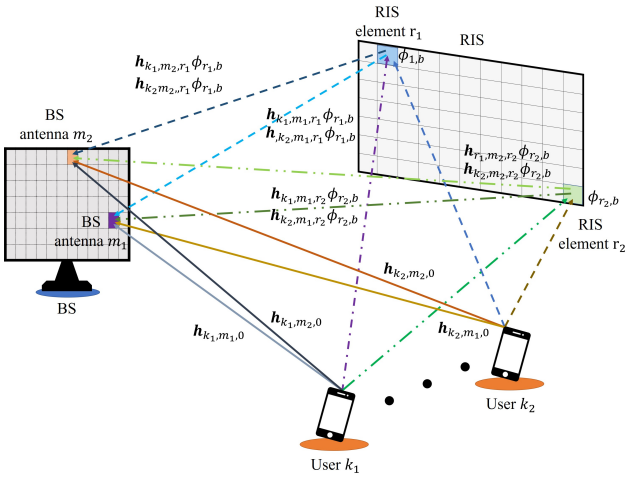

Fig. 1: RIS-aided system comprised of a multiple-antenna BS and K single-antenna users.

Notation: Lowercase bold symbols denote column vectors; uppercase bold symbols denote matrices. Superscripts $(\cdot)^{\mathrm{T}}$, $(\cdot)^{\mathrm{H}}$ and $(\cdot)^{-1}$ denote matrix transpose, Hermitian transpose, and inversion operations, respectively. $\boldsymbol{I}_a$, $\mathbf{0}_{1\times q}$ and $\mathbf{0}_{p\times q}$ denote an $a \times a$ identity matrix, an $1 \times q$ zero vector and a $p \times q$ zero matrix, respectively. $\mathrm{diag}\{\boldsymbol{x}\}$ denotes a diagonal matrix with diagonal entries equal to those of vector $\boldsymbol{x}$. $\|\boldsymbol{A}\|$ denotes the Frobenius norm of the matrix $\boldsymbol{A}$. $((a))_b$ denotes the operation of a modulo b. $\mathbb{E}\{X\}$, $\Re\{c\}$, c^*, $\mathrm{Var}(\cdot)$, $\odot$, ∇, and $\angle$ denote expectation, the real part of a complex number c, omplex conjugate of a complex number c, variance, Hadamard product, gradient, and angle operators, respectively. $\mathbb{Z}$ represents the set of integers.

II. System Model

We consider an RIS-assisted OFDM system with N subcarriers transmitting over frequency-selective fading channels. As shown in Fig. 1, the RIS is deployed to enable uplink (UL) communication from K single-antenna users to a BS equipped with M antennas. The RIS consists of R passive reflecting elements, each of which can independently adjust the phase of the reflected signal. BS antennas are closely collocated and share the same frequency oscillator. Therefore, the transmission between a given user k and any BS antenna exhibits the same CFO; we denote this CFO by ϵ_k (note that this is independent of the BS antenna index m).

Between each user and each BS antenna, there is one direct path from the user to the BS antenna and there are also R reflected paths via the RIS elements. Therefore, the total

number of channel paths between any user and any BS antenna is $R+1$. We assume that all channels exhibit frequency-selective fading and that the baseband equivalent channels between the users and the BS have a delay spread of at most L samples. $\boldsymbol{g}_{k,m,r} = [g_{k,m,r}(0), g_{k,m,r}(1), \ldots, g_{k,m,r}(L-1)]^{\mathrm{T}}$ represents the CIR from user k to BS antenna m via RIS element r. Also, $\boldsymbol{g}_{k,m,0}$ represents the CIR of the direct link from user k to BS antenna m. $\boldsymbol{h}_{k,m,r} = \boldsymbol{F}_{N,L}\boldsymbol{g}_{k,m,r} = [h_{k,m,r}(0), h_{k,m,r}(1), \ldots, h_{k,m,r}(N-1)]^{\mathrm{T}}$ represents the corresponding channel frequency response (CFR), where $\boldsymbol{F}_N = [\boldsymbol{f}_0, \boldsymbol{f}_1, \ldots, \boldsymbol{f}_{N-1}]$ denotes the $N \times N$ unitary discrete Fourier transform (DFT) matrix, whose elements are given as $[\boldsymbol{F}_N]_{p,q} = \frac{1}{\sqrt{N}} e^{-j\frac{2\pi pq}{N}}$ for $p, q \in \{0, 1, \ldots, N-1\}$ and $\boldsymbol{F}_{N,L} = [\boldsymbol{f}_0, \boldsymbol{f}_1, \ldots, \boldsymbol{f}_{L-1}]$. Here, $\boldsymbol{h}_{k,m,0}$ represents the CFR of the direct link from user k to BS antenna m. For $r \neq 0$, $\boldsymbol{h}_{k,m,r} = \tilde{\boldsymbol{h}}_{k,r} \odot \bar{\boldsymbol{h}}_{m,r}$ denotes the equivalent cascaded CFR of the reflecting link, where $\tilde{\boldsymbol{h}}_{k,r}$ and $\bar{\boldsymbol{h}}_{m,r}$ denote the channel between user k and RIS element r and the channel between BS antenna m and RIS element r, respectively.

In order to estimate the $KM(R+1)$ channel response vectors, the pilot sequence frame is divided into $R+1$ blocks. In pilot block $b \in \{0, 1, \ldots, R\}$, the RIS reflection coefficient vector $\boldsymbol{\phi}_b = [\phi_{0,b}, \phi_{1,b}, \ldots, \phi_{R,b}]^{\mathrm{T}}$ is assigned. Path 0 represents the direct path which corresponds to an RIS reflection coefficient of unity, i.e., $\phi_{0,b} = 1$ for all b. In this paper, we assume ideal (i.e., lossless) signal reflection, which means $|\phi_{r,b}| = 1$ for all r and b. The corresponding RIS reflection coefficient matrix is denoted by $\boldsymbol{\Phi} = [\boldsymbol{\phi}_0, \boldsymbol{\phi}_1, \ldots, \boldsymbol{\phi}_R]$.

In pilot block b, user k transmits the time-domain pilot sequence $\boldsymbol{x}_{k,b} = [x_{k,b}(0), x_{k,b}(1), \ldots, x_{k,b}(N-1)]^{\mathrm{T}}$. This vector is the OFDM modulated signal, where OFDM modulation can be represented as the multiplication of the inverse discrete Fourier transform (IDFT) matrix by the frequency-domain pilot vector. The corresponding frequency-domain pilot signal is defined as $\boldsymbol{s}_{k,b} = \boldsymbol{F}_N \boldsymbol{x}_{k,b} = [s_{k,b}(0), s_{k,b}(1), \ldots, s_{k,b}(N-1)]^{\mathrm{T}}$. At the transmitter of user k, a CP of length L_{CP} is added to the time-domain sequence, i.e., $x_{k,b}(u) = x_{k,b}(u+N)$ for $-L_{\mathrm{CP}} \leq u \leq -1$. We consider the CP to be long enough to accommodate small timing offsets between different user signals, i.e., the users are quasi-synchronous in time. The resulting time-domain signal is transmitted to the BS. After the CP removal, sample u of the time-domain received signal at BS antenna m in pilot block b can be written as [22]

$$\begin{aligned} y_{m,b}(u) &= \sum_{k=1}^{K} \sum_{r=0}^{R} \sum_{l=0}^{L-1} e^{j\frac{2\pi\epsilon_k(bL_{\mathrm{s}}+u)}{N}} x_{k,b}(((u-l))_N) \\ &\quad \times g_{k,m,r}(l)\phi_{r,b} + v_{m,b}(u) \\ &= \sum_{k=1}^{K} e^{j\frac{2\pi\epsilon_k(bL_{\mathrm{s}}+u)}{N}} \widetilde{y}_{k,m,b}(u) + v_{m,b}(u), \end{aligned} \tag{1}$$

where $\epsilon_k \in (-0.5, 0.5]$ denotes the CFO for user k normalized by the subcarrier spacing, $L_{\mathrm{s}} = L_{\mathrm{CP}} + N$, $\widetilde{y}_{k,m,b}(u) = \sum_{l=0}^{L-1} x_{k,b}(((u-l))_N)\bar{g}_{k,m,b}(l)$, $\bar{g}_{k,m,b}(l) = \sum_{r=0}^{R} g_{k,m,r}(l)\phi_{r,b}$, and $v_{m,b}(u)$ is time-domain circularly-symmetric complex additive white Gaussian noise (AWGN) having zero mean and variance σ^2. Also, we define vectors $\boldsymbol{y}_{m,b} = [y_{m,b}(0), y_{m,b}(1), \ldots, y_{m,b}(N-1)]^{\mathrm{T}}$ for each m, b.

After discarding the CP and performing an N-point DFT operation on the received signal at each BS antenna, the corresponding frequency-domain received signal at BS antenna m on subcarrier n for pilot block b can be written as [22]

$$\begin{aligned} r_{m,b}(n) = &\sum_{k=1}^{K} \sum_{r=0}^{R} \sum_{p=0}^{N-1} e^{j\frac{2\pi\epsilon_k bL_{\mathrm{s}}}{N}} s_{k,b}(p) f_{\mathrm{s}}(p-n+\epsilon_k) \\ &\times h_{k,m,r}(p)\phi_{r,b} + w_{m,b}(n), \end{aligned} \tag{2}$$

where $f_{\mathrm{s}}(a) = \frac{\sin(\pi a)}{N\sin(\pi a/N)} e^{j\pi(N-1)a/N}$ represents the CFO effect in the frequency domain, $\boldsymbol{w}_{m,b} = \boldsymbol{F}_N \boldsymbol{v}_{m,b} = [w_{m,b}(0), w_{m,b}(1), \ldots, w_{m,b}(N-1)]^{\mathrm{T}}$, and $\boldsymbol{v}_{m,b} = [v_{m,b}(0), v_{m,b}(1), \ldots, v_{m,b}(N-1)]^{\mathrm{T}}$. Consequently, the frequency-domain received vector at BS antenna m for pilot block b can be written as $\boldsymbol{r}_{m,b} = [r_{m,b}(0), r_{m,b}(1), \ldots, r_{m,b}(N-1)]^{\mathrm{T}}$.

III. CFO Effect on Channel Estimation

In this section, we provide a brief overview of two prominent channel estimation methods for RIS-assisted systems in the multi-user scenario. We demonstrate that for these methods, even small CFO values can significantly affect the channel estimation performance.

A. CIR estimation method using OFDMA [14]

A frequency-domain least-squares (LS) channel estimation method for an RIS-aided multi-user OFDMA system without any CFOs was proposed in [14]. In this subsection, we will investigate the effect of CFO on the performance of this method. We begin by providing a brief summary of the method of [14] as follows. In order to avoid MUI, disjoint pilot tone allocations are utilized for all users, i.e., each subcarrier at each block is allocated to only one user. The same number of subcarriers $N_{\mathrm{s}} = N/K \in \mathbb{Z}$ is assigned to each user. Also, the authors of [14] assume $N_{\mathrm{s}} = L$ as the minimum required number of subcarriers assigned to one user. The authors consider equal transmit power allocation for each user over the assigned subcarrier subset for pilot block b. Moreover, equal power is allocated to each subcarrier.

For $N_{\mathrm{s}} = L$ and an interleaved pilot allocation as in [14], the frequency-domain pilot symbol vector from user k for pilot block b after subcarrier mapping can be rewritten as [14, eq. (3)]

$$\boldsymbol{s}_{k,b} = \boldsymbol{\Gamma}_{k,b}\tilde{\boldsymbol{s}}_{k,b}, \tag{3}$$

where $\tilde{\boldsymbol{s}}_{k,b} = [\tilde{s}_{k,b}(0), \tilde{s}_{k,b}(1), \ldots, \tilde{s}_{k,b}(L-1)]^{\mathrm{T}}$ represents the frequency-domain pilot sequence of length L from user k for pilot block b and $\boldsymbol{\Gamma}_{k,b}$ is the $N \times L$ subcarrier allocation matrix of user k for pilot block b. $\boldsymbol{\Gamma}_{k,b}$ is comprised of the columns of the identity matrix whose indices belong to the subcarrier set assigned to user k [14]. Because of the disjoint pilot tone allocations, the received signal vectors for user k at BS antenna m can be written as [14, eq. (7)]

$$\boldsymbol{r}_{k,m,b} = \boldsymbol{\Gamma}_{k,b}^{\mathrm{T}} \boldsymbol{r}_{m,b}. \tag{4}$$

Here, the authors of [14] assume that the same disjoint pilot tones and pilot sequences are assigned over all pilot blocks,

i.e., $\mathbf{\Gamma}_{k,b} = \mathbf{\Gamma}_k$ and $\boldsymbol{s}_{k,b} = \boldsymbol{s}_k$ for all b (consequently, $\boldsymbol{r}_{k,m,b} = \boldsymbol{r}_{k,m}$). By using disjoint pilot tone allocations, the CIR matrix for each user can be individually estimated [14].

When $\epsilon_k = 0$ for all k, the received signal vector (4) can be written as [14, eq. (7)]

$$\begin{aligned}\boldsymbol{r}_{k,m,b} =& \mathbf{\Gamma}_k^{\mathrm{T}} \boldsymbol{r}_{m,b} \\ =& \mathbf{\Gamma}_k^{\mathrm{T}} \operatorname{diag}\{\tilde{\boldsymbol{s}}_k\} \boldsymbol{H}_{k,m} \boldsymbol{\phi}_b + \widetilde{\boldsymbol{w}}_{k,m,b} \\ =& \operatorname{diag}\{\tilde{\boldsymbol{s}}_k\} \boldsymbol{F}_{N,L} \boldsymbol{G}_{k,m} \boldsymbol{\phi}_b + \widetilde{\boldsymbol{w}}_{k,m,b} \\ =& \mathbf{\Lambda}_k \boldsymbol{G}_{k,m} \boldsymbol{\phi}_b + \widetilde{\boldsymbol{w}}_{k,m,b},\end{aligned} \tag{5}$$

where $\boldsymbol{H}_{k,m} = \boldsymbol{F}_{N,L} \boldsymbol{G}_{k,m} = [\boldsymbol{h}_{k,m,0}, \boldsymbol{h}_{k,m,1}, \ldots, \boldsymbol{h}_{k,m,R}]$, $\boldsymbol{G}_{k,m} = [\boldsymbol{g}_{k,m,0}, \boldsymbol{g}_{k,m,1}, \ldots, \boldsymbol{g}_{k,m,R}]$, $\widetilde{\boldsymbol{w}}_{k,m,b} = \mathbf{\Gamma}_k \boldsymbol{w}_{m,b}$, $\boldsymbol{w}_{m,b} = [w_{m,b}(0), w_{m,b}(1), \ldots, w_{m,b}(N-1)]^{\mathrm{T}}$, and $\mathbf{\Lambda}_k = \operatorname{diag}\{\tilde{\boldsymbol{s}}_k\} \boldsymbol{F}_{N,L}$. When $\operatorname{rank}(\mathbf{\Lambda}_k) = L$, i.e., $N_{\mathrm{s}} \geq L$, the estimate of $\tilde{\boldsymbol{g}}_{k,m,b} = \boldsymbol{G}_{k,m} \boldsymbol{\phi}_b$ can be obtained as [14, eq. (9)]

$$\widehat{\tilde{\boldsymbol{g}}}_{k,m,b} = \mathbf{\Lambda}_k^{\dagger} \boldsymbol{r}_{k,m,b}, \tag{6}$$

where $\mathbf{\Lambda}_k^{\dagger} = (\mathbf{\Lambda}_k^{\mathrm{H}} \mathbf{\Lambda}_k)^{-1} \mathbf{\Lambda}_k^{\mathrm{H}}$ denotes the left pseudo-inverse of $\mathbf{\Lambda}_k$. By stacking $\widehat{\tilde{\boldsymbol{g}}}_{k,m,b}$ over b, we obtain $\widehat{\widetilde{\boldsymbol{G}}}_{k,m} = [\widehat{\tilde{\boldsymbol{g}}}_{k,m,0}, \widehat{\tilde{\boldsymbol{g}}}_{k,m,1}, \ldots, \widehat{\tilde{\boldsymbol{g}}}_{k,m,R}] = \boldsymbol{G}_{k,m} \mathbf{\Phi} + \widetilde{W}_{k,m}$, where $\widetilde{W}_{k,m} = [\widetilde{w}_{k,m,0}, \widetilde{w}_{k,m,1}, \ldots, \widetilde{w}_{k,m,R}]$. $\boldsymbol{G}_{k,m}$ can be estimated as [14, eq. (9)]

$$\hat{\boldsymbol{G}}_{k,m} = \widehat{\widetilde{\boldsymbol{G}}}_{k,m} \mathbf{\Phi}^{-1}. \tag{7}$$

In order to minimize the estimation MSE, the matrix $\mathbf{\Phi}$ is required to satisfy $\mathbf{\Phi}^H \mathbf{\Phi} = (R+1) \boldsymbol{I}_{R+1}$, which implies that the reflection pattern matrix is an orthogonal matrix with each entry satisfying the unit-modulus constraint [13]–[15].

However, the above-described method does not consider CFOs. In the following, we investigate the effect of CFOs on the OFDMA-based CIR estimation method of [14]. Since the CFOs break the orthogonality of the subcarriers, there will be MUI from other users when we estimate the channels for user k. In the presence of multiple CFOs, the received signal vectors for user k at BS antenna m can be obtained as

$$\begin{aligned}\boldsymbol{r}_{k,m,b} =& \ \mathbf{\Gamma}_{k,b}^{\mathrm{T}} \boldsymbol{r}_{m,b} \\ =& \mathbf{\Gamma}_k^{\mathrm{T}} \sum_{q=1}^{K} e^{j \frac{2\pi \epsilon_q b L_{\mathrm{s}}}{N}} \mathbf{\Pi}_q \mathbf{\Gamma}_q \operatorname{diag}\{\tilde{\boldsymbol{s}}_q\} \boldsymbol{H}_{q,m} \boldsymbol{\phi}_b + \widetilde{\boldsymbol{w}}_{k,m,b} \\ =& \mathbf{\Gamma}_k^{\mathrm{T}} \sum_{q=1}^{K} e^{j \frac{2\pi \epsilon_q b L_{\mathrm{s}}}{N}} \mathbf{\Pi}_q \mathbf{\Gamma}_q \operatorname{diag}\{\tilde{\boldsymbol{s}}_q\} \boldsymbol{F}_{N,L} \boldsymbol{G}_{m,b} \boldsymbol{\phi}_b + \widetilde{\boldsymbol{w}}_{k,m,b},\end{aligned} \tag{8}$$

where $\mathbf{\Pi}_q$ is a circulant matrix with first row equal to $[f_{\mathrm{s}}(\epsilon_q), f_{\mathrm{s}}(\epsilon_q - 1), \ldots, f_{\mathrm{s}}(\epsilon_q - N + 1)]^{\mathrm{T}}$.

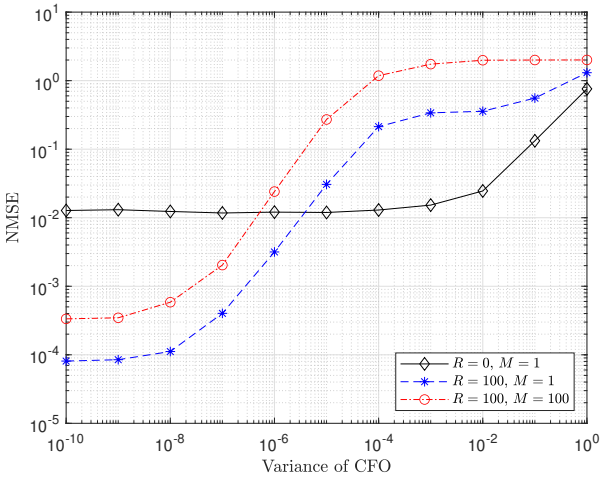

Fig. 2: NMSE performance of the CIR estimation method of [14] as a function of the CFO variance, for different values of M and R. Here the SNR is 10 dB, $L = 32$, and $K = 3$.

In the presence of CFO, however, the estimate of $\tilde{\boldsymbol{g}}_{k,m,b}$ is given by

$$\begin{aligned}\widehat{\tilde{\boldsymbol{g}}}_{k,m,b} =& \ \mathbf{\Lambda}_k^{\dagger} \boldsymbol{r}_{k,m,b} \\ =& \mathbf{\Lambda}_k^{\dagger} \mathbf{\Gamma}_k \mathbf{\Pi}_k \mathbf{\Gamma}_{k,b} \operatorname{diag}\{\boldsymbol{s}_{\mathrm{L,k}}\} \boldsymbol{F}_{N,L} e^{j \frac{2\pi \epsilon_k b L_{\mathrm{s}}}{N}} \bar{\boldsymbol{g}}_{k,m,b} \\ &+ \sum_{q=1, q \neq k}^{K} \mathbf{\Pi}_q \mathbf{\Gamma}_{q,b} \operatorname{diag}\{\boldsymbol{s}_{\mathrm{L,q}}\} \boldsymbol{F}_{N,L} e^{j \frac{2\pi \epsilon_q b L_{\mathrm{s}}}{N}} \bar{\boldsymbol{g}}_{q,m,b} \\ &+ \mathbf{\Lambda}_k^{\dagger} \widetilde{\boldsymbol{w}}_{k,m,b} \\ =& (\boldsymbol{I}_L + \mathbf{\Delta}_{\Lambda,k}) e^{j \frac{2\pi \epsilon_k b L_{\mathrm{s}}}{N}} \bar{\boldsymbol{g}}_{k,m,b} + \boldsymbol{\delta}_{\mathrm{MUI,k}} + \mathbf{\Lambda}_k^{\dagger} \widetilde{\boldsymbol{w}}_{k,m,b} \\ =& e^{j \frac{2\pi \epsilon_k b L_{\mathrm{s}}}{N}} \bar{\boldsymbol{g}}_{k,m,b} + \boldsymbol{\varpi}_{k,m,b},\end{aligned} \tag{9}$$

where $\boldsymbol{\varpi}_k = \mathbf{\Delta}_{\Lambda,k} e^{j \frac{2\pi \epsilon_k b L_{\mathrm{s}}}{N}} \bar{\boldsymbol{g}}_{k,m,b} + \boldsymbol{\delta}_{\mathrm{MUI,k}} + \mathbf{\Lambda}_k^{\dagger} \widetilde{\boldsymbol{w}}_{k,m,b}$ is the total error vector of length L which includes both an interference term *and* a noise term for user k (in contrast to (6), which only includes a noise term). Here, the error matrix of size $L \times L$, which causes ICI for user k (due to $\mathbf{\Pi}_k$) is defined as $\mathbf{\Delta}_{\Lambda,k} = \mathbf{\Lambda}_k^{\dagger} \mathbf{\Pi}_k \mathbf{\Gamma}_k \operatorname{diag}\{\boldsymbol{s}_k\} \boldsymbol{F}_{N,L} - \boldsymbol{I}_L$. $\boldsymbol{\delta}_{\mathrm{MUI,k}}$ is a vector of size $L \times 1$ which models MUI appearing the signal of user k from other users (due to $\mathbf{\Pi}_q$, where $q \neq k$).

Consequently, the CIR matrix for user k at BS antenna m is estimated as

$$\widehat{\boldsymbol{G}}_{k,m} = \widehat{\widetilde{\boldsymbol{G}}}_{k,m} \mathbf{\Phi}^{-1} = \boldsymbol{G}_{k,m} \widetilde{\mathbf{\Phi}} \mathbf{\Phi}^{-1} + \mathbf{\Omega}_{k,m} \mathbf{\Phi}^{-1}, \tag{10}$$

where $\widehat{\widetilde{\boldsymbol{G}}}_{k,m} = [\widehat{\tilde{\boldsymbol{g}}}_{k,m,0}, \widehat{\tilde{\boldsymbol{g}}}_{k,m,1}, \ldots, \widehat{\tilde{\boldsymbol{g}}}_{k,m,R}]$, $\widetilde{\mathbf{\Phi}} = [\boldsymbol{\phi}_0, e^{j \frac{2\pi \epsilon_k L_{\mathrm{s}}}{N}} \boldsymbol{\phi}_1, \ldots, e^{j \frac{2\pi \epsilon_k R L_{\mathrm{s}}}{N}} \boldsymbol{\phi}_R]$, and $\mathbf{\Omega}_{k,m} = [\boldsymbol{\varpi}_{k,m,0}, \boldsymbol{\varpi}_{k,m,1}, \ldots, \boldsymbol{\varpi}_{k,m,R}]$.

In Fig. 2, the NMSE performance of the CIR estimation method using OFDMA is shown as a function of the variance of the CFOs (this variance is assumed to be the same for each CFO) when signal-to-ratio (SNR) is 10 dB. Here, we define NMSE as $\mathbb{E}\|\boldsymbol{G}_{k,m} - \hat{\boldsymbol{G}}_{k,m}\|^2 / K \|\boldsymbol{G}_{k,m}\|^2$. As mentioned earlier, for this numerical result, the interleaved subcarrier allocation is utilized. It can be seen from Fig. 2

that while the NMSE performance is relatively robust to CFO for the system without RIS ($R = 0$), the performance of the RIS-aided system (illustrated for $R = 100$) is much more sensitive to CFO, and even a relatively small value of the CFO variance can significantly degrade the accuracy of the channel estimation method of [14]. Note that a CFO variance of 10^{-4} corresponds to CFOs in the range of 10^{-2}, which has been shown in the OFDM literature to have little effect on the system performance [23]. Also, this detrimental effect of CFOs on the NMSE performance of the RIS-aided system becomes even more pronounced as the number of BS antennas increases (illustrated for $M = 100$). The reasons for this behavior are as follows: 1) when $\epsilon_k \neq 0$, the term $e^{j2\pi\epsilon_q bL_{\mathrm{S}}/N}$ in $\widetilde{\boldsymbol{\Phi}}$ disables accurate estimation of $\boldsymbol{G}_{k,m}$, since $\widetilde{\boldsymbol{\Phi}}\boldsymbol{\Phi}^{-1} \neq \boldsymbol{I}_{R+1}$; and 2) ICI and MUI, besides the noise, are absorbed into $\boldsymbol{\Omega}_{k,m}\boldsymbol{\Phi}^{-1}$, so that the error terms in (10) degrade the accuracy more substantially than when there is only the noise term. Consequently, the entire set of all CFOs needs to be estimated and compensated.

B. Joint CFO and CIR estimation method of [15] used with TDMA

As shown in the previous subsection, the MUI caused by CFOs can severely degrade the performance of CIR estimation in OFDMA systems. To tackle this issue, TDMA pilot sequences can be employed and CFO/channel estimation performed in the time domain; such a joint CFO and CIR estimation method was proposed in [15] for a single-user scenario. One pilot block is divided into K non-overlapping time slots of length $\bar{N} = N/K$. It is assumed that $\bar{N} \geq 2L$. Time slot k is assigned to user k, and users transmit pilot sequences only in their assigned time slots (i.e., TDMA). For time slot k in pilot block b, user k transmits a length-$\bar{N}$ periodic pilot sequence of period L, i.e., $x_{k,b}(u+L) = x_{k,b}(u)$ for $u \in \{2(k-1)\bar{N}, 2(k-1)\bar{N}+1, \ldots, 2k\bar{N}-L-1\}$.

With this pilot structure, we can extend the joint CFO and CIR estimation method in [15] from the single-user scenario to the multi-user scenario. For discrete time $u \in \{2(k-1)\bar{N} + L-1, 2(k-1)\bar{N}+L, \ldots, 2k\bar{N}-1\}$ in pilot block b, the transmission of user k does not exhibit any MUI when the length of each time slot is longer than $2L$. This means that the total overhead length is at least $2KL(R+1)$. Since the number of reflection elements R is usually large even for a moderately sized RIS, the resulting channel estimates can easily become outdated. Therefore, it is worth noting that when N is fixed, the system of [15] with TDMA can support only half the number of users compared to the system of [14] (for [14], $K_{\max} = N/L$, while for [15] with TDMA, $K_{\max} = N/2L$). Consequently, a joint CFO and CIR estimation method with high pilot resource efficiency is required for RIS-aided multi-user massive MIMO OFDM systems, which outperforms these existing approaches.

IV. Proposed Joint CFO and CIR Estimation Method

In this section, we describe the proposed joint CFO and channel estimation method for OFDM-based RIS-aided multi-user massive MIMO systems. First, we present the proposed pilot structure, then we present the proposed joint CFO and CIR estimation method. Finally, we derive a closed-form expression for the channel estimation MSE, which is subsequently used to prove that the proposed pilot structure minimizes this MSE.

			$b=0$			$b=1$			$b=2$			$b=3$			⋯
$\tilde{n}$	u	k	1	2	3	1	2	3	1	2	3	1	2	3	⋯
1	0		0	0	1	1	0	0	0	1	0	0	0	1	⋯
	1		0	0	0	0	0	0	0	0	0	0	0	0	⋯
	2		0	0	0	0	0	0	0	0	0	0	0	0	⋯
	3		0	0	0	0	0	0	0	0	0	0	0	0	⋯
2	4		0	1	0	0	0	1	1	0	0	0	1	0	⋯
	5		0	0	0	0	0	0	0	0	0	0	0	0	⋯
	6		0	0	0	0	0	0	0	0	0	0	0	0	⋯
	7		0	0	0	0	0	0	0	0	0	0	0	0	⋯
3	8		1	0	0	0	1	0	0	0	1	1	0	0	⋯
	9		0	0	0	0	0	0	0	0	0	0	0	0	⋯
	10		0	0	0	0	0	0	0	0	0	0	0	0	⋯
	11		0	0	0	0	0	0	0	0	0	0	0	0	⋯

Fig. 3: Proposed pilot structure in the time domain when $K = 3$ and $L = 4$.

A. Proposed transmit sequence structure

As shown in the previous section, the CFOs cannot be ignored when performing channel estimation for RIS-aided networks. Also, since a long pilot overhead is required for channel estimation, it is undesirable to use existing CFO estimation methods for non-RIS-aided networks. This is because such methods require additional pilot overhead. However, it is difficult to individually extract each CFO from the received signal in (1). Also, because the overhead length for channel estimation changes linearly with the number of RIS elements (which in turn is usually large in practical applications), it is not desirable to use more resources than $KL(R+1)$.

In the following, we propose an impulsive pilot sequence which requires $KL(R+1)$ pilot resources (here, we assume that $N = KL$). As it will be shown in Section IV-B, the proposed pilot can be used for both CFO and CIR estimation. For simplicity, we assume that $(R+1)/K \in \mathbb{Z}$.

As shown in Fig. 3, for pilot block b, user k transmits a pilot sequence of length N, $\boldsymbol{x}_{k,b} = [x_{k,b}(0),\ x_{k,b}(1),\ \ldots,\ x_{k,b}(N-1)]^{\mathrm{T}}$. Vector $\boldsymbol{x}_{k,b}$ is the column vector corresponding to the pair (k,b) in Fig. 3. $x_{k,b}(u)$ is assigned as

$$x_{k,b}(u) = \begin{cases} 1, & u = ((L(b-k)))_N \\ 0, & \text{otherwise} \end{cases}. \tag{11}$$

If, for each pilot block b, the pilot sequence $\boldsymbol{x}_{k,b}$ is divided into K sub-slots of length L, i.e.,

$$\boldsymbol{x}_{k,b} = \begin{bmatrix} \boldsymbol{x}_{k,b,1}^{\mathrm{T}} & \boldsymbol{x}_{k,b,2}^{\mathrm{T}} & \cdots & \boldsymbol{x}_{k,b,K}^{\mathrm{T}} \end{bmatrix}^{\mathrm{T}}, \tag{12}$$

where $\boldsymbol{x}_{k,b,\widetilde{n}} = [x_{k,b,\widetilde{n}}, 0, \ldots, 0]^{\mathrm{T}}$, then it can be noted that the pilot sequence design in (11) ensures that $x^*_{p,b,\widetilde{n}} x_{q,b,\widetilde{n}} = 0$ when $p \neq q \in \{1, 2, \ldots, K\}$ for all b, and $\widetilde{n}$. Based on the pilot sequence design (11), in each time slot, only one assigned user transmits a pilot symbol. The received pilot sequence in this time slot and its corresponding CP portion are used for CFO estimation. In our proposed CIR estimation method, pilot sequences over all time slots are used.

B. Proposed correlation-based CFO estimation

Based on the pilot sequence design, the received signal (1) at discrete time instant $N-1$ for pilot block b with $((b))_K = k-1$ (i.e., the last sub-slot of the pilot block is assigned for user k) can be rewritten as

$$y_{m,b}(N-1) = e^{j\frac{2\pi\epsilon_k(bL_{\mathrm{s}}+N-1)}{N}} \widetilde{y}_{k,m,b}(N-1) + v_{m,b}(N-1). \tag{13}$$

Due to the CP, $\tilde{y}_{k,m,b}(N-1) = \tilde{y}_{k,m,b}(-1)$ and thus the received signal at time instant -1 can be written as

$$y_{m,b}(-1) = e^{j\frac{2\pi\epsilon_k(bL_{\mathrm{s}}-1)}{N}} \widetilde{y}_{k,m,b}(N-1) + v_{m,b}(-1). \tag{14}$$

Consequently, the correlation of $y_{m,b}(N-1)$ and $y_{m,b}(-1)$ can be obtained as

$$\begin{aligned} c_{k,m,b} =& y^*_{m,b}(-1) y_{m,b}(N-1) \\ =& e^{j2\pi\epsilon_k} \left|\widetilde{y}_{k,m,b}(N-1)\right|^2 + \nu_{k,m,b}(N-1), \end{aligned} \tag{15}$$

where

$$\begin{aligned} \nu_{k,m,b} =& v^*_{m,b}(-1) e^{j\frac{2\pi\epsilon_k(bL_{\mathrm{s}}+N-1)}{N}} \widetilde{y}_{k,m,b}(N-1) \\ &+ e^{-j\frac{2\pi\epsilon_k(bL_{\mathrm{s}}-1)}{N}} \widetilde{y}^*_{k,m,b}(-1) v_{m,b}(N-1) \\ &+ v^*_{m,b}(-1) v_{m,b}(N-1). \end{aligned}$$

Since $x_{k,b}(u)$, $g_{k,m,r}(l)$ and $v_{m,b}(u)$ are independent random variables and $\mathbb{E}\{v_{m,b}\} = 0$, we have $\mathbb{E}\{\nu_{k,m,b}(N-1)\} = 0$ for all k. Therefore, we can mitigate the influence of the noise term $\nu_{k,m,b}$ by averaging the correlation samples over $(R+1)/K$ pilot blocks (recall that $(R+1)/K \in \mathbb{Z}$) and M BS antennas. After sharing the received signals between BS antennas, the CFO of user k can be estimated as

$$\begin{aligned} \hat{\epsilon}_k =& \frac{\angle\left(\frac{K}{M(R+1)} \sum_{m=1}^{M} \sum_{d=1}^{(R+1)/K} c_{k,m,(d-1)K+k-1}\right)}{2\pi} \\ =& \frac{\angle\left(e^{j2\pi\epsilon_k} \breve{y}_k + \bar{\nu}_k\right)}{2\pi}, \end{aligned} \tag{16}$$

where

$$\breve{y}_k = \sum_{m=1}^{M} \sum_{d=1}^{\frac{(R+1)}{K}} \frac{K\left|\widetilde{y}_{k,m,(d-1)K+k-1}(N-1)\right|^2}{M(R+1)},$$

and

$$\bar{\nu}_k = \sum_{m=1}^{M} \sum_{d=1}^{(R+1)/K} \frac{K\nu_{k,m,(d-1)K+k-1}}{M(R+1)}.$$

Since $\mathbb{E}\{\nu_{k,m,b}\}$ is zero, it easily follows that $\mathbb{E}\{\bar{\nu}_{k,m,b}\}$ is also zero. The variance of $\bar{\nu}_k$ can be derived as

$$\begin{aligned} \mathrm{Var}(\bar{\nu}_k) =& \mathrm{Var}\left(\sum_{m=1}^{M} \sum_{d=1}^{(R+1)/K} \frac{K\nu_{k,m,(d-1)K+k-1}}{M(R+1)}\right) \\ =& \sum_{m=1}^{M} \sum_{d=1}^{(R+1)/K} \frac{K^2 \mathrm{Var}(\nu_{k,m,(d-1)K+k-1})}{M^2(R+1)^2} \\ =& \frac{2K\sigma^2 \sum_{m=1}^{M} \sum_{r=0}^{R} \rho_{k,m,r}(L-1)}{M^2(R+1)} + \frac{K\sigma^4}{M(R+1)}, \end{aligned} \tag{17}$$

where $\rho_{k,m,r}(l)$ represents the channel power delay profile (PDP) for $g_{k,m,r}(l)$. Consequently, when M and R are large, the noise term becomes sufficiently small due to the averaging.

C. Proposed CIR estimation

Based on the pilot sequence design, the received signal for pilot block b is also composed of K time slots, i.e., $\boldsymbol{y}_{m,b} = [\boldsymbol{y}^{\mathrm{T}}_{m,b,1}, \boldsymbol{y}^{\mathrm{T}}_{m,b,2}, \ldots, \boldsymbol{y}^{\mathrm{T}}_{m,b,K}]^{\mathrm{T}}$, where $\boldsymbol{y}_{m,b,\widetilde{n}} = [y_{m,b,\widetilde{n}}(0), y_{m,b,\widetilde{n}}(1), \ldots, y_{m,b,\widetilde{n}}(L-1)]^{\mathrm{T}}$ and $\widetilde{n} \in \{1, 2, \ldots, K\}$. Because of the impulsive property of the pilot sequence, the received signal can be rewritten as

$$\begin{aligned} y_{m,b,\widetilde{n}}(l) =& \sum_{k=1}^{K} e^{j\frac{2\pi\epsilon_k(bL_{\mathrm{s}}+(\widetilde{n}-1)L+l)}{N}} \sum_{r=0}^{R} g_{k,m,r}(l)\phi_{r,b} \\ &+ v_{m,b,\widetilde{n}}(l), \end{aligned} \tag{18}$$

where $v_{m,b,\widetilde{n}}(l) = v_{m,b}((\widetilde{n}-1)L + l)$. By vertically stacking $y_{m,b,\widetilde{n}}(l)$ over $\widetilde{n}$, we can obtain

$$\begin{aligned} \boldsymbol{y}_{m,b}(l) &= [y_{m,b,1}(l)\ y_{m,b,2}(l)\ \cdots\ y_{m,b,K}(l)]^{\mathrm{T}} \\ &= \boldsymbol{\Theta}_b(l)\boldsymbol{g}_{\phi,m,b}(l) + \tilde{\boldsymbol{v}}_{m,b}(l), \end{aligned} \tag{19}$$

where $\boldsymbol{g}_{\phi,m,b} = [\sum_{r=0}^{R} g_{1,m,r}(l)\phi_{r,b}, \sum_{r=0}^{R} g_{2,m,r}(l)\phi_{r,b}, \ldots, \sum_{r=0}^{R} g_{1,m,r}(l)\phi_{r,b}]^{\mathrm{T}}$, $\tilde{\boldsymbol{v}}_{m,b}(l) = [v_{m,b,1}(l), v_{m,b,2}(l), \ldots, v_{m,b,K}(l)]^{\mathrm{T}}$, $\boldsymbol{\Theta}_b(l) = [\boldsymbol{\theta}_{b,1}(l), \boldsymbol{\theta}_{b,2}(l), \ldots, \boldsymbol{\theta}_{b,K}(l)]$, and $\boldsymbol{\theta}_{b,k}(l) = [e^{j\frac{2\pi\epsilon_k(bL_{\mathrm{s}}+l)}{N}} x_{k,b,1}, e^{j\frac{2\pi\epsilon_k(bL_{\mathrm{s}}+L+l)}{N}} x_{k,b,2}, \ldots, e^{j\frac{2\pi\epsilon_k(bL_{\mathrm{s}}+(K-1)L+l)}{N}} x_{k,b,K}]^{\mathrm{T}}$. Based on the pilot sequence design, since $\boldsymbol{\Theta}_b$ is always a full-rank square matrix, $\boldsymbol{\Theta}_b$ is invertible. Since $\boldsymbol{\Theta}_b^H \boldsymbol{\Theta}_b = \boldsymbol{I}_N$, we can obtain $\boldsymbol{\Theta}_b^{-1} = \boldsymbol{\Theta}_b^H$.

When the CFO ϵ_k for all users k are known, $\boldsymbol{g}_{\phi,m,b}$ can be estimated as

$$\hat{\boldsymbol{g}}_{\phi,m,b}(l) = \boldsymbol{\Theta}_b^H(l)\boldsymbol{y}_{m,b}(l) = \boldsymbol{g}_{\phi,m,b}(l) + \boldsymbol{\Theta}_b^H(l)\tilde{\boldsymbol{v}}_{m,b}(l). \tag{20}$$

In order to minimize the channel estimation MSE, $\mathbb{E}\{\tilde{\boldsymbol{v}}^H_{m,b}(l)\boldsymbol{\Theta}_b(l)\boldsymbol{\Theta}_b^H(l)\tilde{\boldsymbol{v}}_{m,b}(l)\}$, $\boldsymbol{\Theta}_b(l)$ is required to satisfy $\mathbb{E}\{\boldsymbol{\Theta}_b^H(l)\boldsymbol{\Theta}_b(l)\} = \boldsymbol{I}_K$. It is not easy to guarantee this condition, since the matrix $\boldsymbol{\Theta}_b(l)$ depends on the CFO values which are unknown *a priori*; however, the proposed pilot sequence design in (11) ensures that this property holds. Since

$x^*_{p,b,\tilde{n}} x_{q,b,\tilde{n}} = 0$ for all $\tilde{n}$ when $p \neq \tilde{q} \in \{1, 2, \ldots, K\}$, the expectation of $\boldsymbol{\Theta}_b^H(l)\boldsymbol{\Theta}_b(l)$ can be expressed as

$$\begin{aligned}\mathbb{E}\{\boldsymbol{\Theta}_b^H(l)\boldsymbol{\Theta}_b(l)\} &= \begin{bmatrix}\tilde{\boldsymbol{\theta}}_{b,1}(l) & \tilde{\boldsymbol{\theta}}_{b,2}(l) & \cdots & \tilde{\boldsymbol{\theta}}_{b,K}(l)\end{bmatrix} \\ &= \begin{bmatrix}\sum\limits_{\tilde{n}=1}^{K}|x_{1,b,\tilde{n}}|^2 & 0 & \cdots & 0 \\ 0 & \sum\limits_{\tilde{n}=1}^{K}|x_{2,\tilde{n}}|^2 & \cdots & 0 \\ \vdots & \vdots & \ddots & \vdots \\ 0 & 0 & \cdots & \sum\limits_{\tilde{n}=1}^{K}|x_{K,b,\tilde{n}}|^2\end{bmatrix} \\ &= \boldsymbol{I}_K,\end{aligned} \tag{21}$$

where $\tilde{\theta}_{b,\tilde{n},l}(\epsilon_k - \epsilon_{\tilde{k}}) = e^{j2\pi(\epsilon_k-\epsilon_{\tilde{k}})(bL_{\mathrm{s}}+(\tilde{n}-1)L+l)/N}$ and

$$\tilde{\boldsymbol{\theta}}_{b,k}(l) = \begin{bmatrix}\sum_{\tilde{n}=1}^{K}\mathbb{E}\{\tilde{\theta}_{b,\tilde{n},l}(\epsilon_k-\epsilon_1)\}x^*_{1,b,\tilde{n}}x_{k,b,\tilde{n}} \\ \sum_{\tilde{n}=1}^{K}\mathbb{E}\{\tilde{\theta}_{b,\tilde{n},l}(\epsilon_k-\epsilon_2)\}x^*_{2,b,\tilde{n}}x_{k,b,\tilde{n}} \\ \vdots \\ \sum_{\tilde{n}=1}^{K}\mathbb{E}\{\tilde{\theta}_{b,\tilde{n},l}(\epsilon_k-\epsilon_K)\}x^*_{K,b,\tilde{n}}x_{k,b,\tilde{n}}\end{bmatrix}.$$

After using the CFO estimates $\hat{\epsilon}_k$ for all users k to form the estimate $\widehat{\boldsymbol{\Theta}}_b(l)$ of $\boldsymbol{\Theta}_b(l)$, (20) can be rewritten as

$$\begin{aligned}\hat{\boldsymbol{g}}_{\phi,m,b}(l) =& \widehat{\boldsymbol{\Theta}}_b^H(l)\boldsymbol{y}_{m,b}(l) \\ =& \operatorname{diag}\{\bar{\boldsymbol{\theta}}_{b,l}\}\boldsymbol{G}_m(l)\boldsymbol{\phi}_b + \widehat{\boldsymbol{\Theta}}_b^H(l)\tilde{\boldsymbol{v}}_{m,b}(l) \\ =& \boldsymbol{G}_m(l)\boldsymbol{\phi}_b + \boldsymbol{\gamma}_{m,l,b} + \bar{\boldsymbol{v}}_{m,b}(l) \\ =& \boldsymbol{G}_m(l)\boldsymbol{\phi}_{\epsilon,b} + \check{\boldsymbol{v}}_{m,b}(l),\end{aligned} \tag{22}$$

where $\boldsymbol{\gamma}_{m,l,b} = (\operatorname{diag}\{\bar{\boldsymbol{\theta}}_{b,l}\} - \boldsymbol{I}_K)\boldsymbol{G}_m(l)\boldsymbol{\phi}_b$, $\check{\boldsymbol{v}}_{m,b}(l) = \boldsymbol{\gamma}_{m,l,0} + \bar{\boldsymbol{v}}_{m,b}(l)$, $\bar{\boldsymbol{v}}_{m,b}(l) = \widehat{\boldsymbol{\Theta}}_b^H(l)\tilde{\boldsymbol{v}}_{m,b}(l)$ and

$$\bar{\boldsymbol{\theta}}_{b,l} = \begin{bmatrix}\tilde{\theta}_{b,((K-1+b))_K+1,l}(\epsilon_1-\hat{\epsilon}_1) \\ \tilde{\theta}_{b,((K-2+b))_K+1,l}(\epsilon_2-\hat{\epsilon}_2) \\ \vdots \\ \tilde{\theta}_{b,((b))_K+1,l}(\epsilon_K-\hat{\epsilon}_K)\end{bmatrix}.$$

Consequently, by horizontally stacking $\hat{\boldsymbol{g}}_{\phi,m,b}(l)$ over b, we can estimate $\boldsymbol{G}_m(l) = [\boldsymbol{g}^{\mathrm{T}}_{1,m}(l), \boldsymbol{g}^{\mathrm{T}}_{2,m}(l), \ldots, \boldsymbol{g}^{\mathrm{T}}_{K,m}(l)]^{\mathrm{T}}$, where $\boldsymbol{g}_{K,m}(l) = [g_{k,m,0}(l), g_{k,m,1}(l), \ldots, g_{k,m,R}(l)]$, as

$$\begin{aligned}\hat{\boldsymbol{G}}_m(l) =& \hat{\boldsymbol{G}}_{\phi,m}(l)\boldsymbol{\Phi}^{-1} = \boldsymbol{G}_m(l)\boldsymbol{\Phi}\boldsymbol{\Phi}^{-1} + \check{\boldsymbol{V}}_m(l)\boldsymbol{\Phi}^{-1} \\ =& \boldsymbol{G}_m(l) + \check{\boldsymbol{V}}_m(l)\boldsymbol{\Phi}^{-1},\end{aligned} \tag{23}$$

where $\hat{\boldsymbol{G}}_{\phi,m}(l) = [\hat{\boldsymbol{g}}_{\phi,m,0}(l), \hat{\boldsymbol{g}}_{\phi,m,1}(l), \ldots, \hat{\boldsymbol{g}}_{\phi,m,R}(l)]$, and $\check{\boldsymbol{V}}_m(l) = [\check{\boldsymbol{v}}_{m,0}(l), \check{\boldsymbol{v}}_{m,1}(l), \ldots, \check{\boldsymbol{v}}_{m,R}(l)]$. After repeating (22) to (23) for all l, we can obtain the full CIR matrix $\hat{\boldsymbol{G}}_{k,m}$ for all k.

The MSE of the CIR estimation in (23) can be written as

$$\begin{aligned}\mathbb{E}\{\|\boldsymbol{G}_m(l) - \hat{\boldsymbol{G}}_m(l)\|^2\} =& \mathbb{E}\{\|\check{\boldsymbol{V}}_m(l)\boldsymbol{\Phi}^{-1}\|^2\} \\ =& \mathbb{E}\{\|(\boldsymbol{\Gamma}_{m,l} + \bar{\boldsymbol{V}}_m(l))\boldsymbol{\Phi}^{-1}\|^2\},\end{aligned} \tag{24}$$

where $\boldsymbol{\Gamma}_{m,l} = [\boldsymbol{\gamma}_{m,l,0}, \boldsymbol{\gamma}_{m,l,1}, \ldots, \boldsymbol{\gamma}_{m,l,R}]$. In order to minimize the MSE, the matrix $\boldsymbol{\Phi}$ is chosen to satisfy $\mathbb{E}\{\boldsymbol{\Phi}^H\boldsymbol{\Phi}\} = (R+1)\boldsymbol{I}_{R+1}$, which implies that the reflection pattern matrix can be any kind of a (scaled) unitary matrix (this condition was also shown to be optimal in [13] and [14] for the case of no CFO).

Consequently, since the components of $\boldsymbol{\Gamma}_{m,l}$ and those of $\bar{\boldsymbol{V}}_m(l)$ are independent and the mean of $v_{m,b,p}(l)$ is equal to zero, (24) can be simplified as

$$\begin{aligned}&\sum_{l=0}^{L-1}\mathbb{E}\{\|\boldsymbol{G}_m(l) - \hat{\boldsymbol{G}}_m(l)\|^2\} \\ &= \sum_{l=0}^{L-1}\mathbb{E}\{\|(\boldsymbol{\Gamma}_{m,l} + \bar{\boldsymbol{V}}_m(l))\boldsymbol{\Phi}^{-1}\|^2\} \\ &= \sum_{l=0}^{L-1}\mathbb{E}\{\|(\boldsymbol{\Gamma}_{m,l} + \bar{\boldsymbol{V}}_m(l))^H(\boldsymbol{\Phi}^{-1})^H\boldsymbol{\Phi}^{-1}(\boldsymbol{\Gamma}_{m,l} + \bar{\boldsymbol{V}}_m(l))\|\} \\ &= \sum_{l=0}^{L-1}\frac{\mathbb{E}\{\|(\boldsymbol{\Gamma}^H_{m,l} + \bar{\boldsymbol{V}}_m(l)^H)(\boldsymbol{\Gamma}_{m,l} + \bar{\boldsymbol{V}}_m(l))\|\}}{R+1} \\ &= \sum_{l=0}^{L-1}\frac{\mathbb{E}\{\|\boldsymbol{\Gamma}^H_{m,l}\boldsymbol{\Gamma}_{m,l}\|\}}{R+1} + \sum_{l=0}^{L-1}\frac{\mathbb{E}\{\|\boldsymbol{\Gamma}^H_{m,l}\bar{\boldsymbol{V}}_m(l))\|\}}{R+1} \\ &\quad + \sum_{l=0}^{L-1}\frac{\mathbb{E}\{\|\bar{\boldsymbol{V}}_m(l)^H\boldsymbol{\Gamma}_{m,l}\|\}}{R+1} + \sum_{l=0}^{L-1}\frac{\mathbb{E}\{\|\bar{\boldsymbol{V}}_m(l)^H\bar{\boldsymbol{V}}_m(l))\|\}}{R+1} \\ &= \sum_{l=0}^{L-1}\frac{\mathbb{E}\{\|\boldsymbol{\Gamma}^H_{m,l}\boldsymbol{\Gamma}_{m,l}\|\}}{R+1} + \sum_{l=0}^{L-1}\frac{\mathbb{E}\{\|\bar{\boldsymbol{V}}_m(l)^H\bar{\boldsymbol{V}}_m(l))\|\}}{R+1} \\ &= \sum_{l=0}^{L-1}\frac{\sum_{k=1}^{K}\sum_{r=0}^{R}\Delta_{\epsilon,r,k}(l)\rho_{k,m,r}(l)}{R+1} + KL\sigma^2,\end{aligned} \tag{25}$$

where $\Delta_{\epsilon,b,k}(l) = 2 - 2\cos(2\pi(\epsilon_k - \hat{\epsilon}_k)(bL_{\mathrm{s}} + ((((b))_K - k + 1))_K L + l)/N)$. Here, when $\epsilon_k - \epsilon_k$ is close to 0, $\Delta_{\epsilon,b,k}$ also becomes close to 0. As a result, the MSE is more sensitive to noise than to CFOs. It can be seen that the performance of the proposed CIR estimation method is improved as the CFO estimation accuracy is improved.

V. Computational complexity analysis and comparison

In this section, we analyze and compare the computational complexity of our proposed joint CFO and CIR estimation method with the approach in [15] and the CIR estimation method in [14] in terms of the number of complex multiplications.

The total computational complexity of the proposed method is given by

$$C_{\mathrm{Proposed}} = C_{\mathrm{CFO,Pro}} + C_{\mathrm{CIR,Pro}} = \mathcal{O}(R^3 + KMR^2), \tag{26}$$

where $C_{\mathrm{CFO,Pro}} = \mathcal{O}(MR)$ is the computational complexity of the proposed CFO estimation method (evaluation of (16)), and $C_{\mathrm{CIR,Pro}} = \mathcal{O}(R^3 + KMR^2)$ is the computational complexity of the proposed CIR estimation method (evaluation of (20)–(23) for all l and m).

The computational complexity of the method of [14] (evaluation of (9)–(10)) is given by

$$C_{\mathrm{CIR,OFDMA}} = \mathcal{O}(R^3 + NMR^2 + 2NMR + 3L^2NM). \tag{27}$$

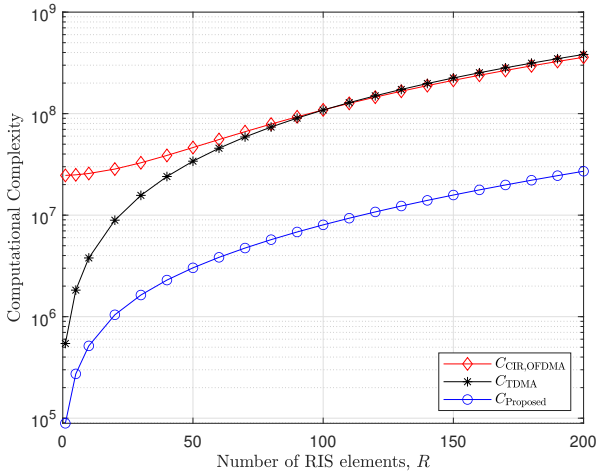

Fig. 4: Computational complexity as a function of R when $K = 5$, $L = 32$, and $M = 50$.

The total computational complexity of the method in [15] is given by

$$\begin{aligned} C_{\text{TDMA}} =& C_{\text{CFO,TDMA}} + C_{\text{CIR,TDMA}} \\ =& \mathcal{O}(R^3 + NMR^2 + LNMR), \end{aligned} \tag{28}$$

where $C_{\text{CFO,TDMA}} = \mathcal{O}(KMR)$ and $C_{\text{CIR,TDMA}} = \mathcal{O}(R^3 + NMR^2 + LNMR)$ are the computational complexity of CFO estimation and CIR estimation, respectively.

Fig. 4 shows the numerical evaluation of the computational complexity of the proposed method and of the (appropriately enhanced) approaches in [14], [15]. As shown in (26) and (28), in the computational complexity of joint CFO and CIR estimation, the computational complexity of CIR estimation is much higher than that of correlation-based CFO estimation. Fig. 4 demonstrates that the proposed method has lower computational complexity than the other methods. When N is a constant and R increases, the computational load for all the methods under study converges: when $R \gg N$, $C_{\text{Proposed}} \approx \mathcal{O}(R^3 + KMR^2)$ and $C_{\text{CIR,OFDMA}} \approx C_{\text{TDMA}} \approx \mathcal{O}(R^3 + NMR^2)$. Consequently, by the use of the proposed method, we can further reduce the computational burden compared to the other approaches as $L = N/K$ increases.

VI. RIS Reflection Coefficient Optimization

In the previous section, it has been demonstrated that the computational complexity of joint CFO and CIR estimation is proportional to R. Similarly, the complexity of optimizing the RIS phase shifts increases rapidly with R, especially when a grid search is utilized. Since R is in general large for RIS-aided systems, the optimization of the RIS phase shifts may require a long time and in some cases can even exceed the coherence time of the channel. Consequently, for RIS-aided systems, it is important to reduce the computational complexity and the execution time, not only for CFO/CIR estimation but also for RIS optimization. Motivated by this, we propose a low-complexity line search method with projected gradients using an adaptive step size for optimizing the RIS reflection coefficients.

A. Problem statement

After estimating the CFO and CIR in the training phase, the RIS reflection coefficients for the data transmission phase need to be optimized in order to maximize the achievable rate in the considered communication system. This problem can be formulated as

$$\text{(P1)}: \max_{\boldsymbol{\phi}_{\text{d}}} f_1(\boldsymbol{\phi}_{\text{d}}) = \frac{\sum_{m=1}^{M}\sum_{k=1}^{K}\sum_{n=0}^{N-1} \log_2\left(1 + \frac{P\widehat{\mathcal{G}}_{k,m,n,\epsilon}(\boldsymbol{\phi}_{\text{d}})}{P\sum_{q=1,q\neq k}^{K}\widehat{\mathcal{G}}_{q,m,n,\epsilon}(\boldsymbol{\phi}_{\text{d}}) + N\Upsilon\sigma^2}\right)}{N + L_{\text{CP}}} \tag{29}$$

$$\text{Subject to } \ |\phi_{\text{d,r}}| = 1 \ \forall\, r = 1, 2, \ldots, R, \tag{30}$$

where

$$\widehat{\mathcal{G}}_{k,m,n,\epsilon}(\boldsymbol{\phi}_{\text{d}}) = \left|\sum_{r=0}^{R}\sum_{p=0}^{N-1} e^{j\frac{2\pi(\epsilon_k - \hat{\epsilon}_k)(R+1)L_{\text{s}}}{N}} f_s(p - n + (\epsilon_k - \hat{\epsilon}_k)) \times \gamma_k(p)\hat{h}_{k,m,r}(n)\phi_{\text{d,r}}\right|^2$$

is the estimated frequency-domain channel gain between user k and BS antenna m on subcarrier n, which varies with the vector of reflection coefficients $\boldsymbol{\phi}_{\text{d}} = [1, \phi_{\text{d},1}, \ldots, \phi_{\text{d,R}}]^{\text{T}}$, and $\Upsilon \geq 1$ denotes the achievable rate gap due to the use of practical modulation and coding schemes.

B. Projected gradient method

Removing the constant denominator, the optimization problem (P1) can be rewritten as

$$\text{(P2)}: \max_{\boldsymbol{\phi}_{\text{d}}} f_2(\boldsymbol{\phi}_{\text{d}}) = \sum_{m=1}^{M}\sum_{k=1}^{K}\sum_{n=0}^{N-1} \ln\left(1 + \frac{P\widehat{\mathcal{G}}_{k,m,n,\epsilon}(\boldsymbol{\phi}_{\text{d}})}{P\sum_{q=1,q\neq k}^{K}\widehat{\mathcal{G}}_{q,m,n,\epsilon}(\boldsymbol{\phi}_{\text{d}}) + N\Upsilon\sigma^2}\right) \tag{31}$$

$$\text{Subject to } \ |\phi_{\text{d,r}}| = 1 \ \forall\, r = 1, 2, \ldots, R. \tag{32}$$

After differentiating $f_2(\boldsymbol{\phi}_{\text{d}})$ with respect to $\boldsymbol{\phi}^*_{\text{d},\tilde{\text{r}}}$ for $\tilde{r} \in \{1, 2, \ldots, R\}$, we obtain

$$\frac{d}{d\phi^*_{\text{d},\tilde{\text{r}}}} f_2(\boldsymbol{\phi}_{\text{d}}) = \sum_{m=1}^{M}\sum_{k=1}^{K}\sum_{n=0}^{N-1} A^{-1}_{m,n} \times \frac{d}{d\phi^*_{\text{d},\tilde{\text{r}}}} \frac{\widehat{\mathcal{G}}_{k,m,n,\epsilon}(\boldsymbol{\phi}_{\text{d}})}{\sum_{q=1,q\neq k}^{K}\widehat{\mathcal{G}}_{q,m,n,\epsilon}(\boldsymbol{\phi}_{\text{d}}) + N\Upsilon\sigma^2/P}, \tag{33}$$

where

$$A_{m,n} = 1 + \frac{\widehat{\mathcal{G}}_{k,m,n,\epsilon}(\boldsymbol{\phi}_{\text{d}})}{\sum_{q=1,q\neq k}^{K}\widehat{\mathcal{G}}_{q,m,n,\epsilon}(\boldsymbol{\phi}_{\text{d}}) + N\Upsilon\sigma^2/P}.$$

Furthermore, we have

$$\begin{aligned}
&\frac{d}{d\phi^*_{\mathrm{d},\tilde{\mathrm{r}}}}\frac{\widehat{\mathcal{G}}_{k,m,n,\epsilon}(\boldsymbol{\phi}_{\mathrm{d}})}{\sum_{q=1,q\neq k}^{K}\widehat{\mathcal{G}}_{q,m,n,\epsilon}(\boldsymbol{\phi}_{\mathrm{d}})+N\Upsilon\sigma^2/P}\\
&=\frac{\frac{d}{d\phi^*_{\mathrm{d},\tilde{\mathrm{r}}}}\widehat{\mathcal{G}}_{k,m,n,\epsilon}(\boldsymbol{\phi}_{\mathrm{d}})(\sum_{q=1,q\neq k}^{K}\widehat{\mathcal{G}}_{q,m,n,\epsilon}(\boldsymbol{\phi}_{\mathrm{d}})+N\Upsilon\sigma^2/P)}{(\sum_{q=1,q\neq k}^{K}\widehat{\mathcal{G}}_{q,m,n,\epsilon}(\boldsymbol{\phi}_{\mathrm{d}})+N\Upsilon\sigma^2/P)^2}\\
&-\frac{\widehat{\mathcal{G}}_{k,m,n,\epsilon}(\boldsymbol{\phi}_{\mathrm{d}})\frac{d}{d\phi^*_{\mathrm{d},\tilde{\mathrm{r}}}}(\sum_{q=1,q\neq k}^{K}\widehat{\mathcal{G}}_{q,m,n,\epsilon}(\boldsymbol{\phi}_{\mathrm{d}})+N\Upsilon\sigma^2/P)}{(\sum_{q=1,q\neq k}^{K}\widehat{\mathcal{G}}_{q,m,n,\epsilon}(\boldsymbol{\phi}_{\mathrm{d}})+N\Upsilon\sigma^2/P)^2}\\
&=\frac{\frac{d}{d\phi^*_{\mathrm{d},\tilde{\mathrm{r}}}}\widehat{\mathcal{G}}_{k,m,n,\epsilon}(\boldsymbol{\phi}_{\mathrm{d}})\sum_{q=1,q\neq k}^{K}\widehat{\mathcal{G}}_{q,m,n,\epsilon}(\boldsymbol{\phi}_{\mathrm{d}})+N\Upsilon\sigma^2/P}{(\sum_{q=1,q\neq k}^{K}\widehat{\mathcal{G}}_{q,m,n,\epsilon}(\boldsymbol{\phi}_{\mathrm{d}})+N\Upsilon\sigma^2/P)^2}\\
&\quad-\frac{\widehat{\mathcal{G}}_{k,m,n,\epsilon}(\boldsymbol{\phi}_{\mathrm{d}})\frac{d}{d\phi^*_{\mathrm{d},\tilde{\mathrm{r}}}}\sum_{q=1,q\neq k}^{K}\widehat{\mathcal{G}}_{q,m,n,\epsilon}(\boldsymbol{\phi}_{\mathrm{d}})}{(\sum_{q=1,q\neq k}^{K}\widehat{\mathcal{G}}_{q,m,n,\epsilon}(\boldsymbol{\phi}_{\mathrm{d}})+N\Upsilon\sigma^2/P)^2}\\
&=B_{k,m,n}\frac{d}{d\phi^*_{\mathrm{d},\tilde{\mathrm{r}}}}\widehat{\mathcal{G}}_{k,m,n,\epsilon}(\boldsymbol{\phi}_{\mathrm{d}})\\
&\quad+\bar{B}_{k,m,n}\frac{d}{d\phi^*_{\mathrm{d},\tilde{\mathrm{r}}}}\sum_{q=1,q\neq k}^{K}\widehat{\mathcal{G}}_{q,m,n,\epsilon}(\boldsymbol{\phi}_{\mathrm{d}})\\
&=B_{k,m,n}\\
&\quad\times\sum_{r=0}^{R}\sum_{p_1=0}^{N-1}f_s(p_1-n+(\epsilon_k-\hat{\epsilon}_k))\gamma_k(p_1)\hat{h}_{k,m,r}(n)\phi_{\mathrm{d,r}}\\
&\quad\times\sum_{p_2=0}^{N-1}f_s^*(p_2-n+(\epsilon_k-\hat{\epsilon}_k))\gamma_k^*(p_2)\hat{h}^*_{k,m,\tilde{r}}(n)\\
&\quad+\bar{B}_{k,m,n}\sum_{q=1,q\neq k}^{K}\sum_{r=0}^{R}\sum_{p_3=0}^{N-1}f_s(p_3-n+(\epsilon_q-\hat{\epsilon}_q))\\
&\quad\times\gamma_q(p_1)\hat{h}_{q,m,r}(n)\phi_{\mathrm{d,r}}\\
&\quad\times\sum_{p_4=0}^{N-1}f_s^*(p_4-n+(\epsilon_q-\hat{\epsilon}_q))\gamma_q^*(p_4)\hat{h}^*_{q,m,\tilde{r}}(n)\\
&=\mathfrak{B}_{k,m,n}\hat{h}^*_{k,m,\tilde{r}}(n)+\sum_{q=1,q\neq k}^{K}\bar{\mathfrak{B}}_{k,q,m,n}\hat{h}^*_{q,m,\tilde{r}}(n),
\end{aligned}\tag{34}$$

where

$$B_{k,m,n}=\frac{\sum_{q=1,q\neq k}^{K}\widehat{\mathcal{G}}_{q,m,n,\epsilon}(\boldsymbol{\phi}_{\mathrm{d}})+N\Upsilon\sigma^2/P}{(\sum_{q=1,q\neq k}^{K}\widehat{\mathcal{G}}_{q,m,n,\epsilon}(\boldsymbol{\phi}_{\mathrm{d}})+N\Upsilon\sigma^2/P)^2},$$

$$\bar{B}_{k,m,n}=-\frac{\widehat{\mathcal{G}}_{k,m,n,\epsilon}(\boldsymbol{\phi}_{\mathrm{d}})}{(\sum_{q=1,q\neq k}^{K}\widehat{\mathcal{G}}_{q,m,n,\epsilon}(\boldsymbol{\phi}_{\mathrm{d}})+N\Upsilon\sigma^2/P)^2},$$

$$\begin{aligned}
\mathfrak{B}_{k,m,n}=&B_{k,m,n}\sum_{r=0}^{R}\sum_{p_1=0}^{N-1}\sum_{p_2=0}^{N-1}f_s(p_1-n+(\epsilon_k-\hat{\epsilon}_k))\gamma_k(p_1)\\
&\times\hat{h}_{k,m,r}(n)\phi_{\mathrm{d,r}}f_s^*(p_2-n+(\epsilon_k-\hat{\epsilon}_k))\gamma_k^*(p_2),
\end{aligned}$$

and

$$\begin{aligned}
\bar{\mathfrak{B}}_{k,q,m,n}=&\bar{B}_{k,m,n}\sum_{r=0}^{R}\sum_{p_3=0}^{N-1}\sum_{p_4=0}^{N-1}f_s(p_3-n+(\epsilon_q-\hat{\epsilon}_q))\gamma_q(p_1)\\
&\times\hat{h}_{q,m,r}(n)\phi_{\mathrm{d,r}}f_s^*(p_4-n+(\epsilon_q-\hat{\epsilon}_q))\gamma_q^*(p_4).
\end{aligned}$$

Substituting (34) into (33), we obtain

$$\begin{aligned}
\frac{d}{d\phi^*_{\mathrm{d},\tilde{\mathrm{r}}}}f_2(\boldsymbol{\phi}_{\mathrm{d}})=&\sum_{m=1}^{M}\sum_{k=1}^{K}\sum_{n=0}^{N-1}A^{-1}_{m,n}\mathfrak{B}_{k,m,n}\hat{h}^*_{k,m,\tilde{r}}(n)\\
&+\sum_{m=1}^{M}\sum_{k=1}^{K}\sum_{n=0}^{N-1}A^{-1}_{m,n}\sum_{q=1,q\neq k}^{K}\bar{\mathfrak{B}}_{k,q,m,n}\hat{h}^*_{q,m,\tilde{r}}(n).
\end{aligned}\tag{35}$$

The gradient of $f_2(\boldsymbol{\phi}_{\mathrm{d}})$ with respect to $\boldsymbol{\phi}^*_{\mathrm{d}}$ can be written as

$$\begin{aligned}
\nabla_{\boldsymbol{\phi}^*_{\mathrm{d}}}f_2(\boldsymbol{\phi}_{\mathrm{d}})=&\left[\frac{df_2(\boldsymbol{\phi}_{\mathrm{d}})}{d\phi^*_{\mathrm{d},1}},\frac{df_2(\boldsymbol{\phi}_{\mathrm{d}})}{d\phi^*_{\mathrm{d},2}},\cdots,\frac{df_2(\boldsymbol{\phi}_{\mathrm{d}})}{d\phi^*_{\mathrm{d,R}}}\right]^{\mathrm{T}}\\
=&\sum_{m=1}^{M}\sum_{k=1}^{K}\sum_{n=0}^{N-1}A^{-1}_{m,n}\\
&\times\begin{bmatrix}\mathfrak{B}_{k,m,n}\hat{h}^*_{k,m,1}(n)+\sum_{q=1,q\neq k}^{K}\mathfrak{B}_{k,q,m,n}\hat{h}^*_{q,m,1}(n)\\ \mathfrak{B}_{k,m,n}\hat{h}^*_{k,m,2}(n)+\sum_{q=1,q\neq k}^{K}\mathfrak{B}_{k,q,m,n}\hat{h}^*_{q,m,2}(n)\\ \vdots\\ \mathfrak{B}_{k,m,n}\hat{h}^*_{k,m,R}(n)+\sum_{q=1,q\neq k}^{K}\mathfrak{B}_{k,q,m,n}\hat{h}^*_{q,m,R}(n)\end{bmatrix}.
\end{aligned}\tag{36}$$

After computing the gradient above, we update the value of $\boldsymbol{\phi}_{\mathrm{d}}$ in iteration τ according to

$$\boldsymbol{\phi}_{\mathrm{d}}^{(\tau+1)}=P\left(\boldsymbol{\phi}_{\mathrm{d}}^{(\tau)}+\mu\nabla_{\boldsymbol{\phi}^*_{\mathrm{d}}}f_3(\boldsymbol{\phi}_{\mathrm{d}}^{(\tau)})\right),\tag{37}$$

where $\tau\in\{1,2,\ldots,N_\tau\}$ and μ are the iteration index and the step size, respectively, N_τ is the number of iterations, and $P(\cdot)$ is the projection operator. The gradient projection $\tilde{\phi}^{(\tau)}_{\mathrm{d,r}}=P\left(\phi^{(\tau)}_{\mathrm{d,r}}\right)$ is given by

$$\tilde{\phi}^{(\tau)}_{\mathrm{d,r}}=\begin{cases}\phi^{(\tau)}_{\mathrm{d,r}}/|\phi^{(\tau)}_{\mathrm{d,r}}|, & \text{for } \phi^{(\tau)}_{\mathrm{d,r}}\neq 0\\ e^{j\alpha}, & \text{for } \phi^{(\tau)}_{\mathrm{d,r}}=0\end{cases},\tag{38}$$

where $\alpha\in[0,2\pi]$. Consequently, we simultaneously optimize all the RIS reflection coefficients in each iteration of the proposed algorithm.

In order to make the proposed algorithm both computationally efficient and time efficient, we use a line search procedure to adjust the step size μ. The step size μ in (37) can be found as $\mu_0\varrho^{k_\tau}$, where k_τ is the smallest non-negative integer such that $f_3\left(\boldsymbol{\phi}_{\mathrm{d}}^{(\tau+1)}\right)-f_3\left(\boldsymbol{\phi}_{\mathrm{d}}^{(\tau)}\right)\geq\delta_\phi\left\|\boldsymbol{\phi}_{\mathrm{d}}^{(\tau+1)}-\boldsymbol{\phi}_{\mathrm{d}}^{(\tau)}\right\|^2$, where $\mu_0>0$ is the initial value of μ, $\delta_\phi>0$ is a small constant, and $\varrho\in(0,1)$ [24]. The proposed PGM procedure ensures that the objective sequence increases after each iteration. Thus, the PGM is guaranteed to converge to a stationary point of (31), which is, however, not necessarily a globally optimal solution. Consequently, we can optimize the RIS reflection coefficient vector $\boldsymbol{\phi}_{\mathrm{d}}$ using the proposed PGM with a low complexity.

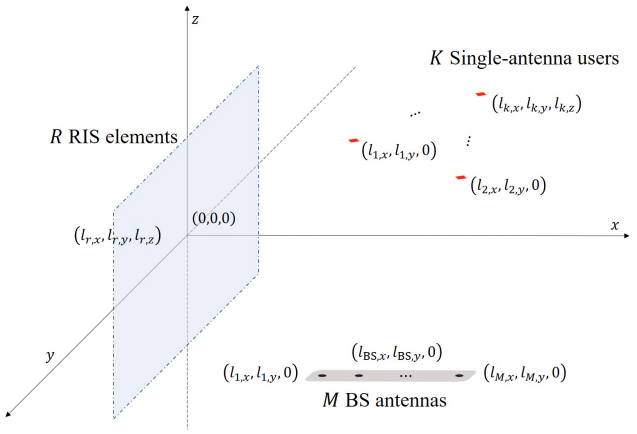

Fig. 5: 3D representation of the BS antennas, the users and the RIS.

VII. Numerical Results and Discussion

In this section, we evaluate the performance of the proposed joint CFO and CIR estimation method. As shown in Fig. 5, M BS antennas, K single-antenna users, and R RIS elements are considered in a three-dimensional (3D) Cartesian coordinate system. The RIS is located in the yz-plane and the position of its midpoint is $(0, 0, 0)$. We assume that the RIS elements are placed in a uniform rectangular array (URA). The distance between the centers of adjacent RIS elements in both y- and z-dimensions is Δ_{RIS}. The BS antennas are placed in a uniform linear array (ULA). For simplicity, we assume here that the BS antennas are located in the xy-plane, where $x, y \geq 0$, and its ULA is parallel to the x-axis. The position of its midpoint is set as $(l_{\mathrm{BS,x}}, l_{\mathrm{BS,y}}, 0)$. The distance between the adjacent BS antennas is Δ_{BS}. We consider Δ_{BS} to be equal to $\lambda/2$ to avoid antenna coupling issues or correlated channels for different antennas, where λ denotes the wavelength. For simplicity, we assume that users are also located also in the xy-plane, where $x \geq 0$ and $y \leq 0$. The position of user k is set as $(l_{k,x}, l_{k,y}, 0)$ and we assume that the users' positions are fixed while the CFO and CIR are being estimated. In the following simulations, all of the CIR vectors are modeled according to tapped delay line-D (TDL-D) model in [25]; this is a frequency-selective fading channel model with a delay spread of L. The first tap is set as a deterministic channel component and the remaining taps follow the Rayleigh channel distribution. The value κ is defined as the ratio of the signal power in the dominant first tap channel component over the total scattered power in the remaining channel components. In this paper, we set $\kappa = 4$ dB while setting the CP length to a larger value than L.

The (far-field) free space path loss (FSPL)[1] for the link from user k to the BS is equal to $\rho_k = \frac{256\pi^2 \tilde{d}_{\mathrm{UR},k}^2 \tilde{d}_{\mathrm{RB}}^2}{\mathcal{G}_{\mathrm{t}} \mathcal{G}_{\mathrm{r}} \lambda^4 \cos\theta_{\mathrm{T},k} \cos\theta_{\mathrm{R}}}$ (see Eq. (7) and (9) in [26]), and $\mathcal{G}_{\mathrm{t}}$ and $\mathcal{G}_{\mathrm{r}}$ are the transmit and receive antenna gains, respectively. The values of $\mathcal{G}_{\mathrm{t}}$ and $\mathcal{G}_{\mathrm{r}}$ are set to 2, since we assume that these antennas radiate/sense signals to/from the relevant half space [26]. $\tilde{d}_{\mathrm{UR},k}$ and $\tilde{d}_{\mathrm{RB}}$ are the distance between the antenna of user k and the midpoint of the RIS and the distance between the midpoint of the RIS and the midpoint of the BS. $\theta_{\mathrm{T},k}$ and θ_{R} are the angle between the incident wave propagation direction from user k and the normal to the midpoint of the RIS and the angle between the normal to the midpoint of the RIS and the reflected wave propagation direction to the midpoint of the BS, respectively. We neglect the spatial correlation among the elements of a CIR vector from user k to RIS element r and a CIR vector from RIS element r to BS antenna m for all k, r and m.

As for the simulation setup, we set $f = 6$ GHz (i.e., $\lambda = 45$ cm), $\Delta_{\mathrm{RIS}} = \Delta_{\mathrm{BS}} = \lambda/2 = 22.5$ cm, $(l_{\mathrm{BS,x}}, l_{\mathrm{BS,y}}, 0) = (200\ \mathrm{m}, 200\ \mathrm{m}, 0)$, $(l_{k,x}, l_{k,y}, 0) = (200{+}k{-}1\ \mathrm{m}, -200\ \mathrm{m}, 0)$, $\kappa = 4$ dB, $K = 5$, $L = 32$, $N = KL = 160$, $L_{\mathrm{CP}} = L + 2 = 34$, $\mu_0 = 1000$, $\delta_\phi = 10^{-5}$, and $\varrho = 0.5$. The normalized CFOs to the subcarrier spacing are generated from a uniform distribution within the range $(-0.5, 0.5]$. The results in all figures are averaged over 5000 independent realizations of the channels and CFOs. We provide the NMSE performance, which is given by $\eta_\epsilon = \frac{1}{K}\mathbb{E}\left\{\frac{\|\boldsymbol{\epsilon}-\hat{\boldsymbol{\epsilon}}\|^2}{\|\boldsymbol{\epsilon}\|^2}\right\}$ for CFO estimation, where $\boldsymbol{\epsilon} = [\epsilon_1, \epsilon_2, \ldots, \epsilon_K]^{\mathrm{T}}$ and $\hat{\boldsymbol{\epsilon}} = [\hat{\epsilon}_1, \hat{\epsilon}_2, \ldots, \hat{\epsilon}_K]^{\mathrm{T}}$, and $\eta_{\mathrm{g}} = \frac{1}{MK}\mathbb{E}\left\{\frac{\|\boldsymbol{G}_{k,m}-\widehat{\boldsymbol{G}}_{k,m}\|^2}{\|\boldsymbol{G}_{k,m}\|^2}\right\}$ for CIR estimation.

Since the estimation method in [14] was not originally designed with CFO estimation capabilities, we extend it by adding the following CFO estimation approach. Only one user sends its periodic pilot sequence of period L for CFO estimation. While the pilot sequences for CFO estimation are being transmitted, the RIS reflection coefficients are constant. By correlating the samples between the received pilot sequences assigned for each user, the CFO is estimated as in (16). For a fair comparison, the same number of pilot resources, i.e., $2L(R+1)$, are used for the proposed method and for the method of [14]. The length of the extra overhead is approximately proportional to R. Since a large value of R is used in RIS systems in practice, the additional resources required for CFO estimation can result in the estimates being outdated. Also, the pilot resources required for [15] are double those required for the proposed joint CFO and CIR estimation method. Consequently, the proposed method uses the lowest amount of pilot resources.

Fig. 6 shows the NMSE performance of the proposed CFO estimation method and of the approach in [15] as a function of SNR with different values of R and the same value of $M = 50$. It can be seen that the performance of each method improves with SNR. It can also be observed that the performance gap between the CFO estimation method in [15] and the proposed CFO estimation method is reduced when R becomes larger. When R is sufficiently large, the proposed method shows better performance than the method of [15]. Fig. 7 shows the NMSE performance of the proposed CFO estimation method and of the TDMA-based approach as a function of the number of BS antennas. As shown in Fig. 7, the performance of both CFO estimation methods improves with M. When R and M are small, the TDMA-based approach performs better than the proposed method because the TDMA-based approach

[1]The FPSL is defined with respect to the midpoint of the RIS and that of the BS antenna array. The reason is that the distances between neighboring BS antennas are very small compared to the propagation distances. The same is true for the distances between the neighboring RIS elements.

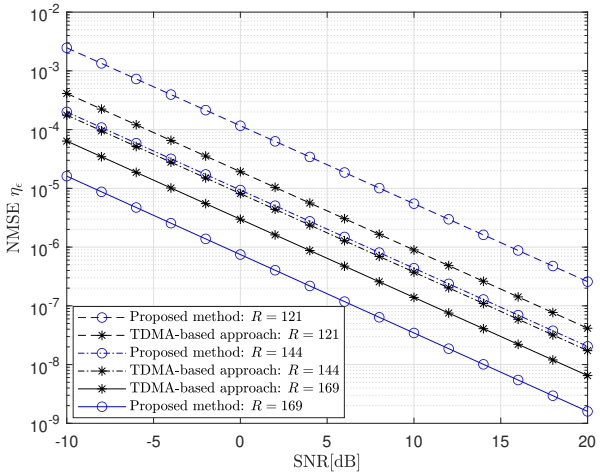

Fig. 6: NMSE performance of the proposed CFO estimation method and of the approach in [15] as a function of SNR, for different values of R when $M = 50$.

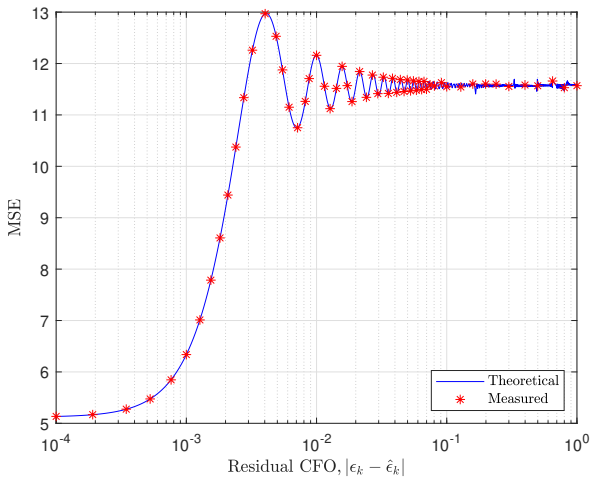

Fig. 8: MSE performance of the proposed CIR estimation method as given by (25) as a function of $|\epsilon_k - \hat{\epsilon}_k|$, when $M = 1$, $R = 64$ and SNR= 10 dB.

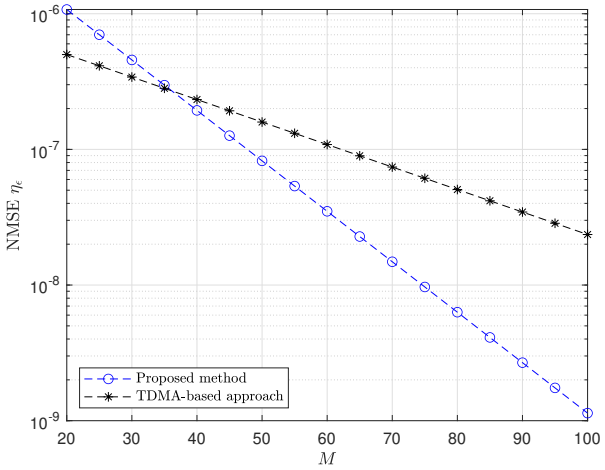

Fig. 7: NMSE performance of the proposed CFO estimation method and of the approach in [15] as a function of M when $R = 169$ and SNR= 10 dB.

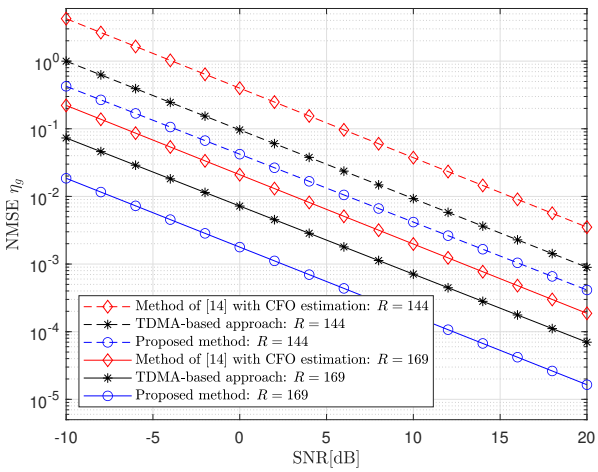

Fig. 9: NMSE performance of the proposed CIR estimation method and of the methods in [14] and [15] as a function of SNR, for different values of R where $M = 50$.

uses more correlation samples (K times that of the proposed method). However, when $R \gg 1$ or $M \gg 1$, as more correlation samples are used, the performance of the proposed method is better than that of the TDMA-based approach. From Fig. 7 it can be observed that the slope of the NMSE curve for the proposed method is about 4-5 times higher than that of the method of [15]. Therefore, if M and R are sufficiently large, the proposed method has a better performance than the method of [15], while using only half of the pilot resources.

Fig. 8 shows the MSE performance of the proposed CIR estimation method as a function of the residual CFO, $|\epsilon_k - \hat{\epsilon}_k|$. In the simulation setup, the parameters are $K = 5$, $L = 32$, $N = KL$, $M = 1$, $R = 64$ and SNR= 10 dB. Since $\bar{\boldsymbol{\theta}}_{b,l}$ in (22) is determined by $\epsilon_k - \hat{\epsilon}_k$, the measured MSE values and the theoretical MSE given by (25) are plotted as a function of $|\epsilon_k - \hat{\epsilon}_k|$. Here we assume for simplicity that the residual CFO values $|\epsilon_k - \hat{\epsilon}_k|$ are equal for all k. It is observed that the measured MSE values match well to the theoretical MSE given by (25). The noise contribution dominates the MSE behavior for small values of residual CFO (eventually converging to MSE $= KL\sigma^2$ as $|\epsilon_k - \hat{\epsilon}_k| \to 0$ for all k). Therefore, the performance of CIR estimation can be improved by enhancing the accuracy of CFO estimation.

Fig. 9 and Fig. 10 show the NMSE performance of different joint CFO and CIR estimation methods for different values of M and R. The NMSE performance of CIR estimation for the proposed method shows better performance than the method in [14], [15]: while the proposed method uses only half of the pilot resources and has a lower computational complexity than the TDMA-based approach in [15]; and because of the extra CFO estimation step, the method of [14] requires more pilot resources than our proposed method. It can be observed

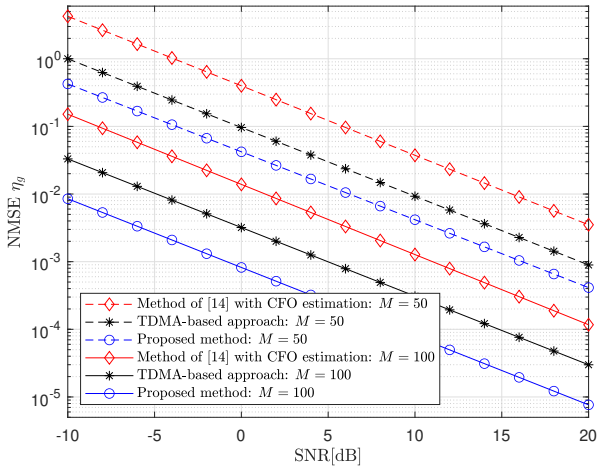

Fig. 10: NMSE performance of the proposed CIR estimation method and of the methods in [14] and [15] as a function of SNR, for different values of M where $R = 144$.

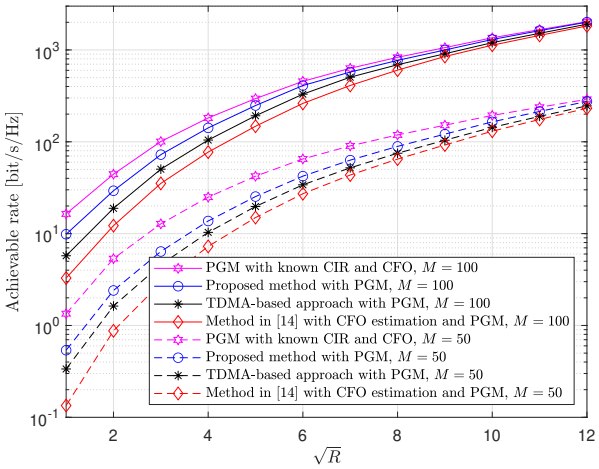

Fig. 12: Achievable rate performance of the methods in [14], [15] and of the proposed joint CFO/CIR estimation method as a function of R with different values of M, when SNR$=$ 10 dB.

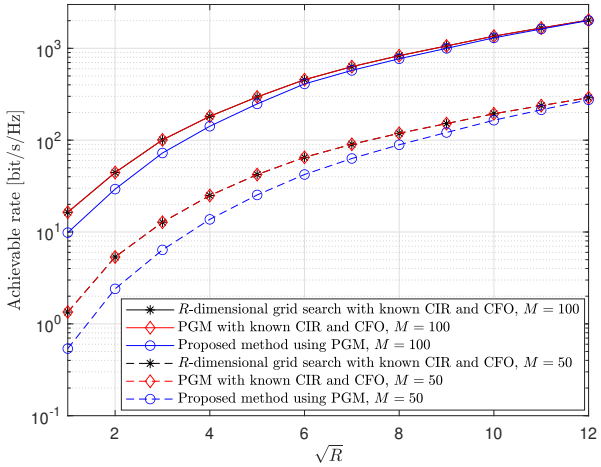

Fig. 11: Achievable rate performance of the proposed PGM as a function of R with different values of M when SNR$=$ 10 dB.

that the CIR estimation performance of the proposed method improves further with the increase of M and R compared to other methods. This is because the CFO estimation accuracy improves as M and R increase, which in turn improves the CIR estimation performance as shown in (25).

Fig. 11 shows the achievable rate performance of the system using the proposed CFO and CIR estimation methods followed by the data transmission phase using the proposed PGM for RIS coefficient optimization (here the SNR is 10 dB). As benchmarks for the proposed PGM, we also plot the optimal achievable rate obtained by using an R-dimensional grid search to maximize (P2) and the achievable rate obtained by the proposed PGM when the CFOs and CIR matrices are assumed to be perfectly known. As shown in Fig. 11, when the CFOs and CIR matrices are accurately estimated, the achievable rate obtained by the proposed PGM is indistinguishable from the optimal achievable rate obtained by the R-dimensional grid search. Also, the achievable rate performance of the proposed PGM with the proposed joint CFO and CIR estimation method becomes close to the optimal achievable rate as M and R increase. This is because when M and R increase, the accuracy of the proposed CFO estimation method increases, and as a result, so does that of the proposed CIR estimation method. Based on this result, the proposed joint CFO and CIR estimation method with the proposed PGM can achieve a close to optimal achievable rate when M and R have large values, which is the case in RIS-aided massive MIMO systems. Also, Fig. 12 shows the achievable rate performance comparison of the proposed joint CFO and CIR estimation method to that of the methods in [14], [15]. Based on the result in Fig. 9, it is observed that as the NMSE performance of CIR estimation improves (i.e., when R increases), the achievable rate performance is close to the optimal achievable rate performance which is obtained by the grid search.

To evaluate the overall performance of the system using both the proposed CFO and CIR estimation method and the proposed PGM, in Fig. 13 we show the bit error rate (BER) performance of the methods in [14] and [15], and of the proposed method as a function of $E_{\rm b}/N_0$, which denotes the ratio of energy per bit to noise power spectral density. In this simulation, $K = 5$, $M = 100$, $R = 144$, and $L = 32$. In the CFO and CIR estimation phase, the methods in [14], [15] and the proposed method use $L(K+2)(R+1)$, $2KL(R+1)$, and $KL(R+1)$ pilot resources, respectively. Using the proposed PGM with $\widehat{\boldsymbol{G}}_{k,m}$ obtained by each estimation method, the RIS reflection coefficient vector $\boldsymbol{\phi}_{\rm d}$ is optimized. In the data transmission phase, the K users send 16-ary PSK modulated OFDMA symbols of length N/K for $R+1$ blocks. Here an interleaved subcarrier allocation for each user is utilized. As shown in Fig. 13, the proposed method shows a better BER performance compared to the methods in [15] and [14]. This

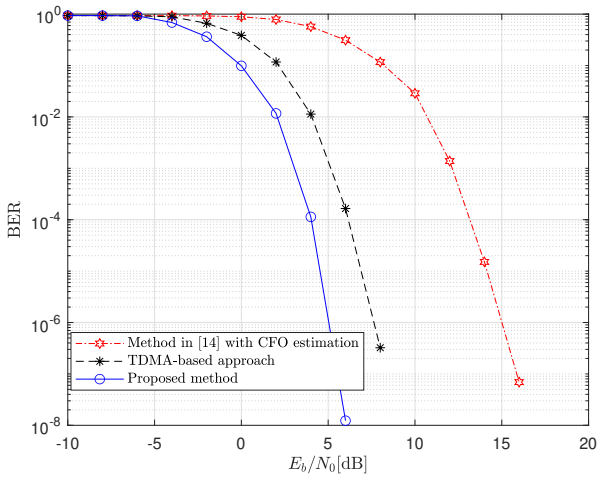

Fig. 13: BER performance of the proposed joint CFO and CIR estimation method compared to that of the approaches of [14] and [15] as a function of E_b/N_0.

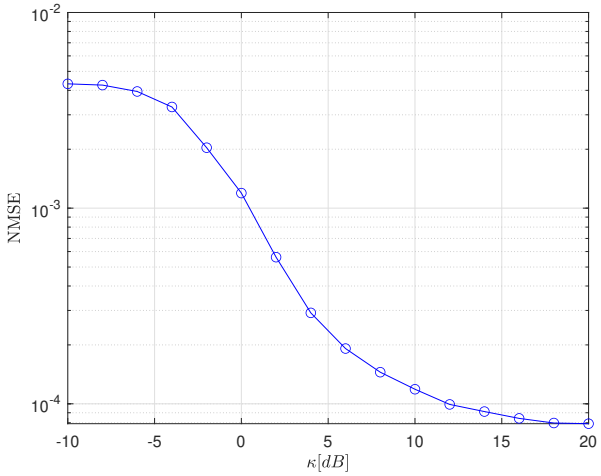

Fig. 14: NMSE performance of the proposed joint CFO and CIR estimation method as a function of κ. Here SNR$=$ 10 dB, $K = 5$, $L = 32$, $M = 100$ and $R = 64$.

trend of the BER performance in Fig. 13 is similar to that of the NMSE performance in Fig. 9 and Fig. 10. The reason is that the error in channel equalization increases as the CIR estimation performance becomes worse. It is worth noting that the proposed method utilizes half the amount of pilot resources than that for the method in [15] and also fewer pilot resources than that of the method of [14].

Fig. 14 shows the NMSE performance for the proposed joint CFO and CIR estimation method as a function of κ, the ratio of the signal power in the dominant first tap channel component over the total scattered power in the remaining channel components. As κ increases, there are three regions: i) a first error floor in the range of $[-10, -4]$ dB; a decreasing region in the range of $[-6, 12]$ dB; and a second error floor in the range of $[14, 20]$ dB. With this result, it is observed that the multi-path interference degrades the NMSE performance of channel estimation. Especially in regions (i) and (ii), the NMSE performance of the proposed CIR estimation method is more influenced by the interference from the non-deterministic channel components than by the noise.

VIII. Conclusion

In this paper, we have demonstrated the deleterious effect of CFO on the NMSE performance of LS-based channel estimation for OFDMA-based RIS-aided multi-user massive MIMO systems. We have proposed, for the first time in the literature, a joint CFO and CIR estimation method for such systems. The proposed pilot structure allows for the estimation of the CFO for each user without MUI. With the obtained CFO estimates and the same pilot resources used for CFO estimation, the CIR matrix is then estimated using LS estimation. It has been demonstrated that the proposed joint estimation method exhibits a better performance in the NMSE and the BER to that of a TDMA-based approach, but requires only half of the pilot overhead. Moreover, the proposed estimation method shows clearly better performance compared to a method using OFDMA while simultaneously requiring a lower overhead. Also, the proposed estimation method has a lower computational complexity than these other approaches. Finally, we proposed a low-complexity PGM for the RIS reflection optimization which provides approximately the same performance as the more computationally demanding grid search method. The proposed methods pave the way for practical deployments of multi-user RIS-assisted large-scale MIMO systems.

References

[1] E. G. Larsson, O. Edfors, F. Tufvesson, and T. L. Marzetta, "Massive MIMO for next generation wireless systems," *IEEE Commun. Mag.*, vol. 52, no. 2, pp. 186–195, 2014.

[2] M. A. Albreem, M. Juntti, and S. Shahabuddin, "Massive MIMO detection techniques: A survey," *IEEE Commun. Surv. Tutor.*, vol. 21, no. 4, pp. 3109–3132, 2019.

[3] J. Zhang, S. Chen, Y. Lin, J. Zheng, B. Ai, and L. Hanzo, "Cell-free massive MIMO: A new next-generation paradigm," *IEEE Access*, vol. 7, pp. 99 878–99 888, 2019.

[4] L. Sanguinetti, E. Björnson, and J. Hoydis, "Toward massive MIMO 2.0: Understanding spatial correlation, interference suppression, and pilot contamination," *IEEE Trans. Commun.*, vol. 68, no. 1, pp. 232–257, Jan. 2020.

[5] E. Basar, M. D. Renzo, J. D. Rosny, M. Debbah, M.-S. Alouini, and R. Zhang, "Wireless communications through reconfigurable intelligent surfaces," *IEEE Access*, vol. 7, pp. 116 753–116 773, 2019.

[6] X. Yuan, Y.-J. A. Zhang, Y. Shi, W. Yan, and H. Liu, "Reconfigurable-intelligent-surface empowered wireless communications: Challenges and opportunities," *IEEE Wirel. Commun.*, vol. 28, no. 2, pp. 136–143, 2021.

[7] N. S. Perović, M. D. Renzo, and M. F. Flanagan, "Channel capacity optimization using reconfigurable intelligent surfaces in indoor mmWave environments," *ICC 2020*, pp. 1–7, June 2020.

[8] N. S. Perović, L. Tran, M. D. Renzo, and M. F. Flanagan, "Achievable rate optimization for MIMO systems with reconfigurable intelligent surfaces," *IEEE Trans. Wirel. Commun.*, vol. 20, no. 6, pp. 3865–3882, 2021.

[9] Q. Wu and R. Zhang, "Intelligent reflecting surface enhanced wireless network via joint active and passive beamforming," *IEEE Trans. Wirel. Commun.*, vol. 18, no. 11, pp. 5394–5409, 2019.

[10] D. Mishra and H. Johansson, "Channel estimation and low-complexity beamforming design for passive intelligent surface assisted MISO wireless energy transfer," *ICASSP 2019*, pp. 4659–4663, 2019.

[11] Y. Yang, B. Zheng, S. Zhang, and R. Zhang, "Intelligent reflecting surface meets OFDM: Protocol design and rate maximization," *IEEE Trans. Commun.*, vol. 68, no. 7, pp. 4522–4535, 2020.

[12] Z.-Q. He and X. Yuan, "Cascaded channel estimation for large intelligent metasurface assisted massive MIMO," *IEEE Wirel. Commun. Lett.*, vol. 9, no. 2, pp. 210–214, 2020.
[13] B. Zheng and R. Zhang, "Intelligent reflecting surface-enhanced OFDM: Channel estimation and reflection optimization," *IEEE Wirel. Commun. Lett.*, vol. 9, no. 4, pp. 518–522, 2020.
[14] B. Zheng, C. You, and R. Zhang, "Intelligent reflecting surface assisted multi-user OFDMA: Channel estimation and training design," *IEEE Trans. Wirel. Commun.*, vol. 19, no. 12, pp. 8315–8329, 2020.
[15] S. Jeong, A. Farhang, N. S. Perović, and M. F. Flanagan, "Low-complexity joint CFO and channel estimation for RIS-aided OFDM systems," *IEEE Wirel. Commun. Lett.*, vol. 11, no. 1, pp. 203–207, 2022.
[16] M. Jung, W. Saad, and G. Kong, "Performance analysis of active large intelligent surfaces (LISs): Uplink spectral efficiency and pilot training," *IEEE Trans. Commun.*, vol. 69, no. 5, pp. 3379–3394, 2021.
[17] H. Liu, X. Yuan, and Y.-J. A. Zhang, "Matrix-calibration-based cascaded channel estimation for reconfigurable intelligent surface assisted multiuser MIMO," *IEEE J. Sel. Areas Commun.*, vol. 38, no. 11, pp. 2621–2636, 2020.
[18] N. K. Kundu and M. R. McKay, "Channel estimation for reconfigurable intelligent surface aided MISO communications: From LMMSE to deep learning solutions," *IEEE Open J. Commun. Soc.*, vol. 2, pp. 471–487, 2021.
[19] A. M. Elbir, A. Papazafeiropoulos, P. Kourtessis, and S. Chatzinotas, "Deep channel learning for large intelligent surfaces aided mm-Wave massive MIMO systems," *IEEE Wirel. Commun. Lett.*, vol. 9, no. 9, pp. 1447–1451, 2020.
[20] A. Taha, M. Alrabeiah, and A. Alkhateeb, "Enabling large intelligent surfaces with compressive sensing and deep learning," *IEEE Access*, vol. 9, pp. 44 304–44 321, 2021.
[21] J. An, C. Xu, L. Gan, and L. Hanzo, "Low-complexity channel estimation and passive beamforming for RIS-assisted MIMO systems relying on discrete phase shifts," *IEEE Trans. Commun.*, vol. 70, no. 2, pp. 1245–1260, 2022.
[22] M. Morelli, C.-C. J. Kuo, and M.-O. Pun, "Synchronization techniques for orthogonal frequency division multiple access (OFDMA): A tutorial review," *Proc. IEEE*, vol. 95, no. 7, pp. 1394–1427, Aug. 2007.
[23] D. Huang and K. Letaief, "An interference-cancellation scheme for carrier frequency offsets correction in OFDMA systems," *IEEE Trans. Commun.*, vol. 53, no. 7, pp. 1155–1165, 2005.
[24] N. S. Perović, L.-N. Tran, M. D. Renzo, and M. F. Flanagan, "Optimization of RIS-aided MIMO systems via the cutoff rate," *IEEE Wirel. Commun. Lett.*, vol. 10, no. 8, pp. 1692–1696, 2021.
[25] 3GPP, "5G; Study on channel model for frequencies from 0.5 to 100 GHz (3GPP TR 38.901 version 14.0.0 Release 14) ," no. 38.901, May 2017, version 14.0.0. [Online]. Available: https://portal.etsi.org/webapp/ewp/copy$_file.asp?wki_id = 52297$
[26] T. Wankai, C. Xiangyu, Z. C. Ming, Y. D. Jun, H. Yu, D. R. Marco, J. Shi, C. Qiang, and J. C. Tie, "Path loss modeling and measurements for reconfigurable intelligent surfaces in the millimeter-wave frequency band," *arXiv preprint, arXiv:2101.08607*, 2021.